The authors want to thank the anonymous referees for the thorough helpful comments. We hope we have been able to satisfy the concerns expressed in these comments and as a result the manuscript has been improved.

Below are the original comments together with our answers.
Colour coding:
- Comments of the referees
- Answers from the authors
- Line or figure in the revised manuscript addressing the comment

Referee #1

1) A table of all the algorithms would be immensely helpful.
We agree with this comment. We have implemented this table, together with accompanying references and explanations in the text.
P18 L11

2) It would be helpful to have a plot of new AMSU-B TWV vs. ECMWF as a function of TWV to show how the errors get worse as you approach the saturation limit of 15 kg/m2 .
Because we did not compare the retrieval with validation data we can only talk about the conclusions from comparing the retrieval with the ECMWF benchmark. The scatter of the retrieval increases when the TWV values increase and we have included a plot in Figure 9 which shows this behaviour. The discussion of this plot has been added to the manuscript.
P24 L12

3) Many of the equations presented in this manuscript are directly in Melsheimer and Heygster (2008) and it may not be necessary to duplicate them here.
In order to introduce the changes implemented in the new algorithm we have to discuss the module specific retrieval equations and we felt that the parameters required for these equations are also necessary (e.g. the calibration parameters, the C_tau functions). With the proper reference in place to the Miao et al. (2001) and Melsheimer and Heygster (2008) we feel that the equations are necessary for the sake of clarity.

4) The authors refer to an “original” algorithm multiple times throughout the manuscript. It should be clarified that this is referring specifically to the Melsheimer and Heygster (2008) algorithm.
We have added a sentence that states that the term “original algorithm” refers specifically to the Melsheimer and Heygster (2008) algorithm and have modified any other occurrence of the term in the text to avoid confusion.
P5 L27

Specific comments:

Abstract:
- You don’t mention what you found. How did the new algorithm perform and what are you general conclusions? This needs to be in the abstract.
The conclusions about extended coverage in the warm months and at higher TWV values over open water with the connected higher uncertainties have been included in the abstract.
P2 L9

Introduction:

- “However this AMSU-B based method...”
Miao et al. (2001) uses SSM/T2. Regardless, please define acronyms the first time they are used.
Corrected the reference to AMSU-B and checked all other undefined acronyms in the text.

- “But the emerging errors were deemed acceptable as a trade-off for extending the retrieval range from 1.5-2 kg/m 2 (for only the three band channels) up to 7 kg/m 2 (for two band channels together with the 150 GHz channel).”
The use of “band channels” to refer to the 183 GHz channel specifically is confusing.
Included the exact frequencies of the channels being referred to in the text for clarity.
P5 L4

- “Melsheimer and Heygster (2008) extends the TWV retrieval range over sea ice
by including the 89 GHz channel into the retrieval.”
Include a short sentence on why including the 89 GHz channel is physically useful (it doesn’t saturate as quickly).
Added a sentence that clarifies that the 183.31 +- 7 GHz channel is the one setting the limit for extended range TWV retrieval. The 89 GHz channel is used because it was next in line of the decreasing frequency channels.
P5 L8

- Much of the paragraph starting at P4 L9 feels like it belongs in section 2.2. Too many technical details for the introduction.
The technical details are also included in Section 2.2, however we feel that the introduction here of the channel frequencies is necessary for describing the state of the art for polar TWV retrieval. The limitations in retrieval range and spatial coverage are dictated by these technical details and the modifications brought on by the new method depend on these details.

- It may be useful to include a statement at the end of the introduction
explaining what will be described in remaining sections (e.g. “Section 2.1
provides a discuss of the RT...”).
Added such a paragraph which describes in short the structure of the manuscript.
P6 L4

Methods

2.1
- Need to make it clear early in the paper that you’re primarily analysing AMSU-B measurements in this study.
Added one sentence that clarifies this aspect.
P6 L16

- “A down-looking microwave radiometer”
You may want to note that this is the same type of instrument as a “humidity sounder”.
Added the note that AMSU-B is a humidity sounder.
P6 L14

2.2

- “In the original paper (Miao, 1998)...”
If this is the original paper that this work is based on, it deserves discussion in the introduction.
This reference points to the PhD dissertation of J. Miao where some of the aspects of TWV retrieval using the 183.31 band channels are discussed for the first time which is why we mention it in the Methods section, but the first retrieval over Antarctica is described in detail in Miao, (2001) which is the original Antarctic paper we discuss in the introduction.
The word “original” has been removed from the sentence to avoid confusion with the other Miao (Miao et al, 2001) paper which describes the Antarctic retrieval.

- “Because the Ts term is the same for both brightness temperatures, it has disappeared from Eq. (2) as a result of the subtraction.”
Technically T_s is still in the b_{ij} term and thus in Eq. (2).
That sentence was removed.

- “To find the relationship between the measured brightness temperature and the water vapour absorption we require the third brightness temperature measured in channel k.”
A brief physical explanation of why three channels are necessary would be appreciated for people unfamiliar with microwave TWV retrievals.
Added a sentence that clarifies the use of the third brightness temperature for obtaining the ratio of brightness temperature differences which is a direct relationship between the measured Tbs and TWV.
P8 L14

- “Compared to the first two terms under the exponent, the quadratic term can be neglected...”
Why? State because it is comparatively small.
Added the clarification that the quadratic term is negligible small compared to the other two.

- “for Arctic atmospheric profiles retrieved from radiosonde measurements.”
Please describe the source of these radiosondes measurements and give a few details.
The radiosonde data come from 27 WMO coastal and island stations in the Arctic, measured between 1996 and 2002. We added this information to the text.
P10 L3

- “W threshold value after which $T_{b,j} \leq T_{b,k}$, or simply...”
A brief physical explanation of why this works would be helpful.
Added the physical explanation for for the Tb channel saturation switch.
P11 L11

2.3

- “The Melsheimer and Heygster (2008) algorithm extension is adapted only for sea ice surfaces.”
Now would be an appropriate time to explain why they didn’t apply it over ocean.
The purpose of the Melsheimer and Heygster (2008) extension was to test this concept out for regions with relatively low TWV (sea ice covered regions) and sea ice surface emissivity data was readily accessible at the time for the required channels. While the use of radiative transfer software for open ocean emissivity simulations is mentioned as a future possibility in that original paper, it was not explored further at the time and we implemented it for this current work. This information has been

added to the text.
P13 L18

- “From the data points over sea ice, the following regression relationship was found...”
Make it clear that this is from Melsheimer and Heygster (2008).

Added a clear reference to the text.
P14 L17

- “The set of four parameters is determined through regression by using simulated brightness temperatures and atmospheric data from radiosonde profiles”
Some detail on how ARTS is used to do this would be helpful.
In Section 2.2 we describe the regression procedure for finding the focal point. With the focal point coordinates known we fit eq. (9) and retrieve the constant calibration parameters C_0 and C_1. Added reference to the proper section in the text.
P15 L14

- “for the L (low TWV), M (mid-TWV) and X (extended-TWV) cases. In the new algorithm, two extra sets of calibration parameters are required, for the M-ow (mid-TWV over open water) and X-ow (extended-TWV over open water) components.”
These nicknames (e.g. “X-ow”) are created but not used in the rest of the manuscript. Either used the shortened names or get rid of them entirely.
The shortened names had to be used in Table I, describing the different retrieval algorithms but besides that they are not used in the rest of the text. They are defined in the table caption and have been removed from the manuscript text.

2.5
- “from radiosondes profiles and simulated brightness temperatures.”
Like was done previously? Please clarify.
This is the same procedure as used in Section 2.3 and initially described in Section 2.2. Because we are describing different sub-algorithms of the retrieval we wanted to emphasize that each module uses its own set of calibration parameters and all are derived using the same procedure (the one described in Section 2.2).
P15 L4

2.6
- “lead to differences in the third significant digit of the C0 and C1 parameters,
which is small compared to other error contributions.”
My interpretation of Fig. 3 is that $C(\tau_j, \tau_k)$ is only important for low values of TWV. But for those low values you’re using an equation without $C(\tau_j, \tau_k)$, so is it ever important? If not, why even bother with the term?
This function has high variability in the low-TWV range of values where the retrieval equation does not include it. In the mid and extended range modules however this function is integrated in the retrieval equation and while it is not constant it does vary slowly with increasing TWV. We show this behavior in Figure 3 in order to back-up our assumption of using one constant value for the function. This constant value is different for the mid and extended range TWV retrieval modules respectively. We have rearranged the order of the sentences in order to clarify that this slow varying function is set to an approximate constant value individually calculated for the mid-TWV as was done for the extended-

TWV in the original Melsheimer and Heygster 2008 paper.
P18 L7

“One of the critical points in the algorithm...”
“to the conditions used in their retrieval...”
“the classical mid-TWV retrieval...”
As there are many algorithms discussed in this manuscript, it’s confusing when you use vague references. Please be clear which algorithm you’re referring to at all times.
Added the convention that the very first TWV retrieval algorithm using humidity sounder measurements by Miao et al. (2001) is referred to as the Antarctic algorithm. The Melsheimer and Heygster (2008) algorithm is referred to as the original algorithm because it represents the original AMSU-B extended range retrieval method from which the new method, the focus of this current work, has been developed. The text has been modified throughout the manuscript to match this convention.

“SSMIS or AMSR-E data...”
Need to define and cite both.
This refers to the ASI sea ice data derived from either SSMIS or AMSR-E measurements. Added a clarification and the ASI reference to the text.
P22 L16

Perhaps consider naming this section “Comparison of results to Melsheimer and Heygster (2008)”, as “previous method” is, again, somewhat vague.
This section was meant to introduce the comparison work done using the new algorithm retrieval. This refers to comparison to the original AMSU-B method as well as the separate (over different spatial domains) inter-comparison with the two AMSR-E products (RSS and NN). The comparison with Melsheimer and Heygster (2008) is now Section 3. Section 2.9 was renamed to “Comparing the new retrieval with other TWV retrieval products” as all products and the spatial and temporal domain over which the comparison is done are introduced here.

“The second dataset is the TWV product from Remote Sensing Systems...”
It would be helpful to mention that these algorithms only work over open ocean. It would also be helpful to give some basic information on the RSS and NN algorithms. What range of TWV can they retrieve? Do they cover the entire Arctic? Do they work over sea or land ice (nope!)?
Added extra details regarding the retrieval ranges and valid spatial domains for both algorithms.
P23 L21

Results and Discussion

3.1

- “Comparing this with the results in Fig. 5 shows that in the months where the contribution of the improved algorithm is greater, the correlation drop is more significant. Most of this contribution represents pixels with large TWV values, close to the retrieval limit that have a higher uncertainty.”
It would be valuable to compare the “original” algorithm and the “new” algorithm to ECMWF for only the pixels where they’re both retrieving TWV. That way you could confirm that the poor correlations in June and September are primarily from the “new” algorithm retrieving over sea ice and open water in regions of high TWV. I also think it would be helpful to see a plot of the “new” retrieved TWV error as a function of the retrieved TWV. That is, quantify how the errors increase as you approach the saturation limit (~15 kg/m 2).

Added three plots (Figure 8) which show the comparison of the two AMSU-B algorithms with each other, and each individually against ECMWF data. By comparing the two algorithms with each other, a plume of data points is visible where the TWV is overestimated by the new algorithm versus the original algorithm. This plume occurs in the extended range TWV domain, with values above 7 kg/m2. This overestimation of some of the data points by the new algorithm is confirmed by the comparison side by side of the new vs ECMWF and original vs ECMWF plots.

- "the highest bias is again seen..."
Figure 6 just shows correlation, not necessarily a bias.
This part is referring to Figure 10 in the revised manuscript which shows bias values between ECMWF and the two AMSU-B retrieval methods.

- "For December there is an increase from −0.06 to −0.3 kg/m 2 ."
This is only because you averaged them. The "Bias New" for all 3 Decembers is closer to zero than "Bias Original" but by averaging you came to the opposite conclusion.

- "Earlier the algorithm was underestimating in both months compared to ECMWF by −0.38..."
June 2007 and June 2008 overestimate and June 2009 underestimates but by averaging you concluded that the algorithm was underestimating for all Junes.

- "Thus, the increase of bias becomes highest in June."
1.86 – (-0.38) = 2.24 and 1.29 – (-1.94) = 3.23 so the increase in bias is actually highest in September.

- Presumably the high bias in the "new" algorithm is due to the addition of retrievals over sea ice and open water. It would be helpful to actually show this. Additionally, do you have a physical explanation for the bias patterns seen in Fig. 7?
All of these errors have been corrected and the discussion on the figure now refers to monthly values and not the averages over the three years.
P26 L28

The question of the high bias in the new algorithm is addressed by the plots in Figure 8 which show that because of the change in switching conditions (discussion in the text) between the original and new algorithm versions, there is a positive bias induced in the extended range TWV domain. The bias patterns in Figure 7 (Figure 10 in the revised version) are explained by the seasonal variability in ice cover and TWV range. In winter the new algorithm uses the dedicated open water modules and retrieves moderate TWV values with very low bias. In summer the original version used the extended range module for retrieving TWV over sea ice and it underestimated because values higher than 15 kg/m2 could be often times retrieved as below this value because of the proximity to the saturation limit. With the new algorithm, **moderately high TWV values (6-8 kg/m2) over open water that were retrieved by the mid-TWV module in the original algorithm have now been passed on to the extended range over open water module in the new algorithm** because of the stricter switch conditions. This module is responsible for the overestimation in summer in the new algorithm retrieved values. This is the only explanation that makes sense to us because this is the only difference between the original and the new algorithm in the spatial domain where both can retrieve valid results. The high TWV over open water regions could not be retrieved in the original algorithm so they are not part of this comparison.
The pixels that were retrieved over open water by the surface independent mid-TWV module at the limits of its sensitivity (because of the relaxed switch condition) are now retrieved by the higher uncertainty extended range open water module in the new algorithm. This more strict switch apparently

leads to lower bias in winter, but higher bias in summer. Because our target is the very low TWV in winter retrieval where no other reliable retrieval algorithms exist, we chose to keep this set up.

3.2

“with the former showing the lowest bias...”
Do you mean the latter? AMSU-B?
The former refers to the AMSR-E based NN approach which scores the lowest bias against ECMWF throughout the entire dataset over the common (all retrieval products) valid spatial domain.

“While the AMSU-B method shows much higher negative bias values in summer it is important to note that average TWV values for the ice-free ocean in the summer months frequently surpass the saturation value of 15 kg/m 2 .”
Is the correct interpretation here that your new AMSU-B algorithm is frequently observing scenes with TWV values of >15 kg/m 2 but still attempts a retrieval and gets values lower than 15 kg/m 2 , resulting in a negative bias? Does this suggest that you need a better method than the one described in section 2 to prevent the algorithm from running on scenes that surpass the saturation value of TWV?

The new AMSU-B algorithm is observing open water (the case for Figure 11) scenes with TWV values of 15 kg/m2 and attempts a retrieval. As the RMSD in this TWV domain is large (> 3 kg/m2) the values that are underestimated will be kept, the retrievals that could result in TWV values above 15 will fail the saturation cut off and will be discarded. Simply put, because of this hard cut off at 15 kg/m2, when the method retrieves values around 15 +- 3 kg/m2, only the underestimated values are retrieved as anything above the limit is discarded. In this sense we consider the switch conditions described in Section 2 as working correctly in moderately to high TWV domains. The disadvantage of this system is that high RMSD retrieval combined with the hard cut off at 15 kg/m2 results in a negative bias when there are many data points to be found in this TWV domain close to the saturation limit.

“Figure 9 top displays the average TWV...”
Might make more sense to show the top panel of Fig. 9 before Fig. 8.
We agree, however we want to show the comparison between the average values in the common valid spatial domain (Fig 12 top) with the existing AMSR-E based retrieval products (only open water) and the average TWV values over the spatial domain where the AMSU-B can retrieve valid data (open water + sea ice cover + land with low enough TWV – Fig. 12 bottom). This represents the key conclusion of this manuscript, that the new AMSU-B method can improve on the original algorithm capabilities for the dry Arctic areas and also provide higher coverage that can match the performance of existing data products in winter months, albeit with reduced performance in summer and in high TWV domains.

“The average retrieved TWV for winter months matches better with the model while the overestimation for summer months, although still present is greatly diminished.”
Is an interpretation of Fig. 9 summer months that:

- Over open ocean, often with high TWV, it does poorly (top panel)

- The bottom panel shows that over all surfaces it does better

- Thus, the bottom panel implies that over sea/land ice the algorithm
must be doing very well compared to ECMWF? If this is a logical interpretation, you should state as

such and include a third panel in Fig. 9 of “New AMSU-B” plotted over ECMWF for only sea and land ice covered regions.

Yes this is a correct interpretation of the results we present, with the comment that over open water the new retrieval does poorly when TWV values are very high (for Arctic standards).
A panel with AMSU-B retrieved TWV versus ECMWF TWV for only sea and land ice covered regions would mean the original AMSU-B algorithm results which are presented in Meslheimer and Heygster (2008). The improvements in the new algorithm are done for the retrieval over open water in the mid-TWV and extended range. As seen in Figure 9 (Figure 12 in the revised manuscript) over open water it matches the performance of the other retrieval products, and in Figure 7 (Figure 10 in the revised manuscript) in winter the new algorithm improves on the bias values for the original algorithm because of the use of the dedicated open water mid-TWV module.

- “This shows the difference between the average atmospheric water vapour load in the dry Central Arctic compared to the ice-free Arctic Ocean areas.”
My understanding is that it technically shows the difference between the entire Arctic and the ice-free Arctic Ocean.
That is correct. We were referring to the big influence (the mean is dragged down) the dry sea ice covered regions of the Arctic have on the average TWV value calculated for the entire Arctic (including all ice free ocean regions above 50N). Changed the wording to better resemble the referee's comment.
P29 L15

- “The previous method was able to retrieve TWV over all surface types for atmospheric water vapour loads up to 6 kg/m 2 and over sea ice for up to 15 kg/m 2 .”
This will be nice to see in a table near the beginning of the paper.
We have added this information to Table I.

Conclusions

- “(Fig. 9, Fig. 4)”
Do you mean Fig. 5 and Fig. 4?
Changed to Figures 4,5 and 12 of the revised manuscript.

- “This difference can be explained by the additional area covered with the new algorithm.”
You could prove this by plotting the original and new AMSU-B vs. ECMWF for matched pixels.
This is now done in Figure 8.

- “This demonstrates the capabilities of the method to retrieve TWV simultaneously over all surface types in the dry atmospheric conditions of the Arctic.”
Well, in the “dry” months you only get ~20% more data with the new algorithm and about the same bias as in the original algorithm. I think the stronger conclusion of this work is that the new algorithm provides greater spatial coverage, primarily in the warmer months, but that the new measurements, often at higher TWV values, have somewhat larger errors.
We agree, and we adapted the text to better match the conclusion of the Referee.

Figures:

- You capitalize “New” and “Original” in many of the figure captions but not in the manuscript. Please be consistent.
Eliminated all capitalized occurrences in the figure captions.

Fig. 3.

- What do the dashed horizontal lines represent?
The dashed horizontal lines represent the variability interval for the C(tau_j,tau_k) parameter inside the TWV range corresponding to each case. Added this sentence to the Figure 3 caption.

Fig. 4

- Here you refer to the “new” algorithm as the “improved” algorithm. Please be consistent in your figures and the manuscript.
Clarified all references to the new algorithm to conform with the naming convention.

- Please make all the text larger.

- Please either make the plots larger or the land/ocean/country border lines thicker.

- The colour for missing data (grey) doesn’t contrast well with the high TWV colour (white). Maybe consider upping the contrast somehow?
In order to match the format of Figure 5, we added examples for the 1st of June and 1st of December 2009 for both original and new algorithms. The colour scale was changed to offer better contrast. Missing data is now white, and the high TWV areas are grey.
Figure 4

Fig. 6

- Dec. 2008 has a much better correlation than the other two Decembers for the “Original” algorithm. Any idea why?
We could not pinpoint any cause for this in the algorithm. This seems to be a natural occurrence specific to 2008 but we do not know why this happens.

Fig. 9

- Make all the text larger.
- Is the bottom panel open ocean and sea ice? Or open ocean, sea ice, and land ice, as stated in the manuscript?
It is open ocean, sea ice and any land surface where TWV value is low enough for the low or mid-TWV modules to work (i.e. below 7 kg/m2).
Figure 12 captions

Technical corrections:
We have implemented all of these technical corrections.

P2 L5: “above-mentioned”
P2 L16: “radiation, and is...”

P3 L27: “fulfill”
We have tried to use British spelling throughout the text.
P4 L6: “Infrared”
P4 L10: “Miao et al. (2001)”
P9 L8: “called the focal point”
P9 L18: New paragraph after “...regression fit.”
P12 L8: “ocean/ice/land”
P12 L13: Don’t start a new paragraph, as you’re still talking about SEPOR/POLEX.
P14 L19: “of the AMSU-B instrument, sea surface temperature, and sea surface roughness...”
P15 L6: “(top panel of Fig. 2)
P15 L7: “following linear relationship in the form of Eq. 19”
P17 L11: “specific”
P18 L24: “Heygster (2008)”
P21 L5: Please cite the ECMWF ERA-Interim.
P22 L9: “new method (Fig. 5).”
P22 L24: “spatial contribution”
P23 L27: “closely follow”
P25 L11: Please define RMS.
P25 L15: “174%”
P26 L2: “high spatial coverage”

Referee #2

General Comments:

I am struggling to interpret Section 3 for a number of reasons:
1) It was not clear that Fig. 5 was not actually a pixel count of the bottom panels on Fig 4, which according to the caption is just an example from 1 day. I think Figs 4 and 5 should be comparable. Perhaps keep the contents of Fig. 4 (the example is nice) and add additional panels for the “new” and “original” algorithms where instead of TWV, the pixels show the frequency of time that a retrieval is possible (perhaps for both January and July 2007-2009). This will provide the spatial context for Fig. 5.
Figure 5 was supposed to show the difference in coverage area as a pixel count between the original and the new method for the whole temporal range we used (2007-2009). We have introduced a new Figure 5 in the revised manuscript which shows the example coverage for the three years in December and June respectively for each of the two algorithms. The retrieval example in Figure 4 has been changed to match the format of Figure 5 with 4 maps, two for each method and for one day in December and one day in June. We agree that this graphical representation supports much better the point about the difference in spatial coverage between the new and original algorithm.

2) You have not explained the domain over which you counted the pixels shown in Fig. 5. I’m assuming that this is the same as was plotted in Fig. 4 (∼ north of 50◦ N) and if so it includes large regions of the north Atlantic and Pacific. It is likely then that a large number of newly-retrievable pixels are found outside the Arctic, which artificially inflates the percent increases reported in Section 3.1. Are you recommending that your method be applied in the north Atlantic and north Pacific too? If I understand correctly, the new algorithm is actually fairly limited in the more southerly parts of the map when averaged over time and these limitations are apparent also in Fig. 4. In addition to quantifying the improvement in coverage from the new algorithm, it would be interesting to know how close to total coverage is represented by the new algorithm. I recommend carefully defining the domain over which

you recommend that algorithm be applied, explain this, and then use this domain to calculate all the results in Section 3.

This comment is partially addressed by the new paragraph added for explaining the revised Figure 5. The domain is the entire Northern Hemisphere where the atmospheric water vapour values fall inside the retrieval range of the algorithm. As an additional complexity, the surface type only matters for the extended range module. While below ~7 kg/m^2 the algorithm can retrieve TWV regardless of the surface type, above this relative threshold the algorithm can only function over open water or sea ice because of the specific reflectivity terms required by this module. This domain of "everything above 50°N" has been used for all of the results in Section 3.

Added more details regarding the geographical domain used for the results in Section 3.

P24 L21

3) I am confused about how to interpret the validation of the retrievals in comparison to the ECMWF data. This is for two main reasons:

> (3a) The ECMWF data are highly dependent on the model, especially at high latitudes, and are thus normally the type of data that is being validated. Therefore, it seems odd to conclude that the retrieval with the smallest systematic difference compared to ECMWF is the best retrieval. This is further confused by the fact that the ECMWF product likely assimilated the same/or similar data to that used in the retrievals. I realize you need a benchmark for comparison, so perhaps this can be resolved by tweaking the wording. What can you conclude through such a comparison?

We agree that ECMWF data does not represent validation level quality but it is a benchmark from which large deviations would signify problems with the retrieval. We see this comparison as a sanity test that could screen obvious deficiencies in the algorithm before more extensive and time consuming validation efforts are undertaken.

Added more details regarding why we chose ECMWF as a benchmark and what was our goal.

P28 L1

> (3b) AMSU-B new and AMSU-B orig are valid over different spatial areas and I assume the same is true for NN and RSS AMSR-E. I don't see where it is explained what spatial areas are averaged for the ECMWF data, but I know that it cannot apply to all four satellite algorithms at the same time. Therefore, it is not possible to isolate systematic differences in retrievals (which is interesting) to biases tied to spatial gaps (which was already established earlier in the section).

For each plot we always used the largest common spatial domain for all methods represented. For Figures 8 and 9 (top) this represents the common domain for all 3 retrieval products and corresponding ECMWF data. All sources were collocated so that the results shown represent the exact same data points coming from the three retrievals. The ECMWF average was calculated for the same number of pixels with collocated model data. This is why there are differences in the ECMWF column heights between Figure 9 top and bottom. The top represents only the open water areas where the AMSR-E based methods (RSS and NN) have valid values while the bottom represents all the areas where the full AMSU-B new algorithm works.

Clarified the methodology for comparing the retrieval products with ECMWF.

P28 L10

4) If the conclusion is that the new algorithm performs poorly compared to existing algorithms, what advantages are there to using it? If biases associated with spatial coverage could be separated from biases in the retrieval perhaps the advantages of the proposed algorithm would become clearer.

Biases associated with coverage are separated from biases in the retrieval. When comparing AMSU-B

new with RSS for example, we are only looking at the open ocean regions above 50◦ N. This means that we are comparing the RSS product with those modules of the AMSU-B retrieval that can function above the ice-free ocean and we can draw conclusions about the performance of these modules. The AMSU-B however is a collection of such modules and the output it produces is one consistent product that covers every region above 50◦ N where the TWV values are below the saturation limit. This includes landmasses where TWV is < ~8 kg/m2 and both sea ice covered and ice-free ocean regions where TWV is <~15 kg/m2. When comparing the new algorithm output with ECMWF data for the same spatial domain, the two agree much better than over open water only. As there are already proven retrieval products that can function over open water, the advantage of the new AMSU-B product lies in the fact that it can seamlessly retrieve over a much larger spatial domain which includes land and sea ice values up to 15 kg/m2 and with higher uncertainty over open water and when TWV values are towards the higher end of its retrieval interval.
Added details in the conclusions about the ranking of the algorithms and the strong points of the new AMSU-B retrieval.
P31 L2

Specific Comments:
P4L19: AMSU-B is introduced here for the first time without explanation. I thought SSM/T2 was the data set being discussed.
Clarified that SSM/T2 is the instrument used in Miao et al (2001) while this work is only based on AMSU-B measurements.
P6 L15

P5L1-10: Can you more clearly articulate your motivation? While I learn later, it is not clear in the introduction why the Melsheimer and Heygster (2008) algorithm is unable to retrieve over the open ocean and marginal ice zone.
The goal of the original paper was to provide an extended range TWV retrieval over sea ice as this was a capability that was missing before, while traditional passive microwave TWV retrievals over open water alone were an operational reality at the time. By only retrieving over high sea ice concentration regions however there are still gaps in the data coverage for the Arctic where the proximity of sea ice prevents open water algorithms to work, while the original AMSU-B algorithm could not retrieve in the extended TWV range if the ice concentration is lower than ~80%. This is where the current work on the new AMSU-B algorithm comes in to close this coverage gap and provide a retrieval solution that is consistent in time and space for the Arctic.
Added these extra details to the manuscript.
P5 L13

Section 2.8: What data set do you use to find the sea ice concentration?
We use collocated ARTIST Sea Ice concentration data (ASI) for deciding the application of open water/sea ice modules. This detail plus the reference was added to the text.
P20 L15

P17L5-13: You have addressed the emissivity difference between 183 and 150 GHz for the ocean component. Why not also develop an analogous correction for the sea ice so that this bias is corrected across the whole Arctic domain?
While the ocean emissivity is relatively well understood and possible to predict with models the treatment of sea ice surface emissivity is more complex. There has been one attempt at applying the emissivity difference correction over sea ice for the mid-range module by using sea ice emissivity data from the same SEPOR/POLEX campaign for the 183 and 150 GHz channels (Selbach, 2003). It was

deemed that the advantages of having one module that is surface independent in the mid-TWV range even with decreased accuracy over some ice surface types outweigh the complexity of implementing a correction for the emissivity difference between 183 and 150 GHz channels.

P3L7-9: “Within this scenario . . .” is a very cumbersome sentence. Consider revising.

We revised the sentence.
P3 L11

P3L11: no comma needed
Done

P4L5: “Satellite retrievals also face. . .”
Done

P4L22: “This assumption is false when switching” to “This is a poor assumption when using”. The sentence is a bit odd anyway. Do you mean that the 183 triplet is used with 150 up to 2 kg/m2 after which one of the 183 bands is saturated and uncertainty increases?
We mean to say that the equal emissivity assumption is valid for the 183 triplet which can retrieve up to 2kg/m2. Above this value one of the 183 bands is saturated and needs to be replaced with the 150 Ghz channel. The new triplet will then use two 183 bands plus the 150 GHz channel and so the equal emissivity assumption is used even though we know that there is a difference in surface emissivities but the resulting increase in uncertainty is deemed acceptable for reasons described at point P17L5-13 above. The sentence was split and simplified.
P4 L26

P5L9: “allows for application of”
Done

Fig 2: It would be better to label the panels as 2a and 2b and refer to them in the text accordingly.
Done
P16L16: You mean for the channels used for retrievals in the mid-range of TWV?
Yes. We have clarified the sentence.

P23L11: “method-specific”
Done

P25L3: “improve the retrieval”
Done

Figs 8 and 9: Please add “new” and “old” to the AMSU-B label in the legends.
In these figures only the new algorithm is presented. The comparison with the two AMSR-E data products is done over open water only and the original AMSU-B algorithm could not retrieve TWV with values above 7 kg/m2 over open water. This would have restricted the common valid spatial domain very much as such low values are encountered in close proximity to sea ice, which is where the two AMSR-E algorithms would not have any valid data.
Specified in the figure captions as well as in the text which spatial domain was used for the comparison.

Manuscript prepared for Atmos. Meas. Tech. Discuss.
with version 4.1 of the LaTeX class copernicus_discussions.cls.
Date: 27 February 2018

Retrieval of Total Water Vapour in the Arctic Using Microwave Humidity Sounders

Raul Cristian Scarlat[1], **Christian Melsheimer**[1] **and Georg Heygster**[1]

[1]Institute of Environmental Physics, University of Bremen, Germany

Correspondence to: Raul Cristian Scarlat
(rauls@iup.physik.uni-bremen.de)

Abstract

Quantitative retrievals of atmospheric water vapour in the Arctic are faced with numerous challenges because of the particular climate characteristics of this area. Here, we attempt to build upon the work of Melsheimer and Heygster (2008) to retrieve total atmospheric water vapour (TWV) in the Arctic from satellite microwave radiometers. While the ~~above mentioned~~ above-mentioned algorithm deals primarily with the ice-covered central Arctic, with this work we are aiming to extend the coverage to low ice cover and ice-free areas. By using modeled values for the microwave emissivity of the ice-free sea surface, we develop two sub-algorithms using different sets of channels that deal solely with open ocean areas. The new algorithm extends the spatial coverage of the retrieval throughout the year but especially in the warmer months when higher TWV values are frequent. The high TWV measurements over both sea ice and open water surfaces are however connected with larger uncertainties as the retrieval values are close to the instrument saturation limits.

This approach allows us to apply the algorithm to regions where previously no data were available and ensures a more consistent physical analysis of the satellite measurements by taking into account the contribution of the surface emissivity to the measured signal.

1 Introduction

Water vapour plays a crucial role within the complex system of our atmosphere. It transports energy from the warmer lower latitudes to higher ones influencing global weather patterns, plays a big part in trapping infrared (IR) radiation, and is highly variable throughout the planetary atmosphere (Le and Gallus Jr, 2012). The water vapour content of air is regulated through the processes of condensation, evaporation and, since the advent of life on this planet, transpiration. These phase changes provide the mechanisms through which water vapour influences atmospheric temperature by adding or removing energy from the air. Through evaporation, energy is stored as latent heat within the water molecules that break away from the liquid as gas, thus leading to a cooling effect in its immediate vicinity. The reverse of this process releases this

latent heat through condensation and provides energy, e.g., for the development of thunderstorm cells.

One of the main characteristics of atmospheric water vapour is its high variability (Trenberth et al., 2005), both in terms of spatial location and temporal evolution. Because of this variability water vapour can be used as an atmospheric tracer that indicates general atmospheric circulation as it accompanies the horizontally moving air masses while its phase changes indicate the location of upwelling or downwelling currents. The average lifetime of a molecule of water in the atmosphere is 10-12 days, during which it can go through many phase changes.

Water vapour is one of the major greenhouse gases in the atmosphere. As such, it is important to monitor the variability of water vapour considering the anthropogenic increase of other greenhouse gases (Solomon et al., 2010). ~~Within the scenario~~ In the context of global warming ~~,~~ the atmosphere's load capacity for water vapour increases and therefore ~~, assuming constant relative humidity, water vapour concentrations would rise, leading to an enhanced greenhouse effect~~ its contribution as the most important greenhouse effect warrants precise monitoring. Model data indicate that this positive feedback loop would increase the sensitivity of surface temperatures to carbon dioxide concentrations by a factor of two (Held and Soden, 2000) ~~,~~ without taking into consideration other possible feedback processes. However, this matter is still debated, as the atmospheric storage of water vapour is not understood well enough to warrant definitive conclusions. In the context of climate change, the importance of water vapour as a greenhouse gas and the positive feedback loop with which it is associated with the global temperature make it necessary to obtain accurate data on atmospheric water vapour load on a global scale.

For the purpose of measurement, we quantify the atmospheric water vapour load as a vertically integrated mass over a column of air with the base area of 1 m^2 and name it as total water vapour or TWV for short. It is the parameter that we will be discussing throughout this paper when referring to measured atmospheric water vapour content.

A reliable method to retrieve atmospheric water vapour content is by using balloon-borne radiosondes. This is an accurate method which provides good vertically resolved measurements. However, these are only point measurements and thus only of local significance (Hurst et al., 2011). Ground-based retrievals such as fixed radiometers and GPS-based retrievals achieve a

lower vertical resolution but are considered feasible for monitoring purposes in regions with a good density of ground stations (Das et al., 2014). However, only satellite measurements fulfil the global coverage requirements of modern numerical weather prediction. Because of the strong absorption properties of water vapour in the infrared and microwave range, suitable space-borne instruments can ensure a complete global coverage of water vapour retrievals (Miao, 1998; Szczodrak et al., 2005; Bobylev et al., 2010).

Radiosonde retrieval of total water vapour in the Arctic is not sufficient because of the scarcity of weather stations in this area. The inhospitable environment presents further challenges to obtain a satisfactory coverage from ground data (Serreze and Hurst, 2000). Satellite ~~retrieval also faces~~ retrievals also face a number of obstacles. ~~Infra-red~~ Infrared measurements are hampered by cloud cover and, while microwave radiometer measurements are a viable option, an incomplete understanding of sea ice emissivity properties challenges retrieval efforts in this area.

One important step towards achieving a satisfying retrieval of TWV in the polar regions came from the work of ~~Miao et al.(2001)~~(Miao et al., 2001). It uses the Special Sensor Microwave/Temperature-2 (SSM/T2) humidity sounder and was designed to work in the Antarctic and will be referred throughout this paper as the Antarctic algorithm, to differentiate it from the other discussed algorithms which were developed for the Arctic. The key concept of this method is the use of several microwave channels with similar surface emissivity but different water vapour absorption behaviour. These are the three channels near the 183.31 GHz water absorption line (183.31$\pm$1,$\pm$3,$\pm$7GHz), which together with the channel at the 150 GHz window frequency allow retrieval of TWV values up to about 7 kg/m^2. Above this value two of the 183.31 GHz band channels become saturated and the sensor fails to 'see' down to the ground anymore. This limit is sufficient for the central Arctic region for most of the year and it shows good agreement with retrievals based on the analysis of GPS signals taken at stations around Antarctica (Vey et al., 2004). However~~this AMSU-B based~~ , because of the limited TWV retrieval range, this method alone cannot ensure a year long monitoring of TWV values (Selbach et al., 2003). ~~The original Antarctic algorithm~~

The Antarctic algorithm (Miao et al., 2001) worked independently of the surface type by assuming the same surface emissivity for all channel frequencies used. ~~This assumption is false~~

~~when switching to~~ While this is a valid assumption for the case when the three 183.31 GHz band channels are used as the surface emissivities are very close to each other, this is a poor assumption when using a triplet that includes the 150 GHz channel (Wang et al., 2001) ~~, but the emerging errors~~ which has a different surface emissivity from the 183.31 GHz bands. The emerging errors from the emissivity differences were deemed acceptable as a trade-off for extending the retrieval range from 1.5-2 kg/m^2 (~~for only the~~ when using all three band channels) up to 7 kg/m^2 (~~for two band channels~~ when using the 183.31±3 and 183.31±7 GHz together with the 150 GHz channel). To improve on this performance the algorithm developed by Melsheimer and Heygster (2008) extends the TWV retrieval range over sea ice by including the 89 GHz channel into the retrieval. Using the triplet of 183.31±7 GHz, 150 GHz and the 89 GHz channels allows the retrieval to function up to the saturation limit of the 183.31±7 GHz channel.

By using the 89 GHz channel, the difference in surface emissivity for the different frequencies becomes too great and the equal emissivity assumption has to be dropped. In order to increase the retrieval range, some information about the emissivity of the ground surface is necessary. Because the surface emissivity of sea ice is very different from that of water, the retrieval algorithm needs to treat each surface type differently. In Melsheimer and Heygster (2008) the priority was to first extend the TWV retrieval range over sea ice as this was a new capability while TWV retrieval algorithms that can function over open water were already operational. After implementing emissivity information about the sea ice surface, the algorithm can retrieve up to 15 kg/m^2 with an error of ≈3 kg/m^2 above sea ice-covered areas. For values below 7 kg/m^2, this algorithm uses the same retrieval mechanism as the ~~original~~ Antarctic algorithm. While providing a boost to the retrieval range of TWV in the Arctic, this method proved the feasibility of using ground emissivity information to achieve passive microwave TWV retrieval over different surface types. In this paper we use the well-understood microwave emissivity of the ice-free sea surface to develop two sub-algorithms for the Melsheimer and Heygster (2008) method that deals solely with open ocean areas. This approach allows ~~applying~~ for application of the extended range algorithm to regions where previously no data were retrievable because of the proximity of sea ice that prevents open water TWV retrieval algorithms to

work or because of the relatively high TWV value that could not be retrieved by the original method over partially ice covered regions. Throughout the rest of this paper we will refer to the Melsheimer and Heygster (2008) algorithm as the original method on which the development of the new algorithm was based on. Because the new algorithm adds additional capabilities, uses modified retrieval equations and increases the complexity of the retrieval we believe the two methods are distinct enough to be compared with each other as stand alone algorithms that use the same working principle.

In Section 2 the basic TWV retrieval in the case of equal surface emissivity is discussed. Following this, we introduce the subsequent extensions to the algorithm starting with the first extension for retrieval over sea ice done by Melsheimer and Heygster (2008) and continuing with the open water extension which is the topic of this current study. Section 3 contains the results of comparing the original retrieval with the new method as well as an intercomparison between the new method and two other retrieval products. In Section 4 the conclusions are presented.

2 Methods

2.1 Radiative transfer equation

As with many other passive microwave retrieval techniques, the algorithm uses a radiative transfer equation to interpret the data from a humidity sounder such as AMSU-B (Advanced Microwave Sounding Unit-B) or MHS (Microwave Humidity Sounder) on board the NOAA (National Oceanic and Atmospheric Administration) 17,18 satellites. Although the method has been tested using the newer MHS instrument data in order to ensure continuity of operation all results presented in this work are based on AMSU-B measurements. A down-looking microwave radiometer, such as the AMSU-B humidity sounder, will measure upward radiances at the top of the atmosphere. They can be expressed as brightness temperatures of the Earth's at-

mosphere. Using the simplified radiative transfer equation from Guissard and Sobiesky (1994), we express the radiance measured by the instruments as the brightness temperature

$$T_b(\theta) = m_p T_s - (T_0 - T_c)(1-\epsilon)e^{-2\tau sec\theta}. \quad (1)$$

Here θ is the off-nadir viewing angle of the satellite, m_p is a correction factor that accounts for the deviation from an isothermal atmosphere and the difference between surface and air temperature. T_s is the surface temperature, T_c the brightness temperature of the cosmic background contribution, and T_0 is the ground level atmospheric temperature. ϵ is the surface emissivity, while τ is the atmospheric opacity. The challenging term here is the correction factor m_p which has to be approximated. For an ideal case of an isothermal atmosphere, the ground being a specular reflector and the surface skin temperature being equal to the ground level atmospheric temperature, m_p would be equal to unity. The Melsheimer and Heygster (2008) algorithm assumes the ground to be a specular reflector which is a sufficient approximation for remote sensing applications in the microwave domain according to Hewison and English (1999).

2.2 The basic idea of TWV retrieval with equal surface emissivity assumption

The entire path leading from the radiative transfer equation and up to the final atmospheric water vapour W retrieval equation has been covered in the ~~original~~ initial Antarctic algorithm paper ~~(Miao et al., 2001)~~ Miao et al. (2001) and in the subsequent Arctic extension paper ~~(Melsheimer and Heygster, 2008)~~Melsheimer and Heygster (2008). We will review it here because the basic mechanism remains the same and is incorporated in the low TWV retrieval component of our final method.

As long as no channel is saturated, i.e., the channel signal still comes from the entire atmospheric column down to the surface and not just the upper layers, all channels "see" the ground and the surface contribution is the same for all three measurements. The water vapour absorption will be different for the three channel frequencies. If i, j, k are the channel indices ordered by decreasing difference to the absorption line maximum then the mass absorption coefficients

κ will be $\kappa_i < \kappa_j < \kappa_k$. To cover the whole retrieval range, the ~~original~~ Antarctic algorithm used two channel triplets

i) 183.31±7, 183.31±3, and 183.31±1 GHz (AMSU-B channels 20, 19, 18); or

ii) 150, 183.31±7, and 183.31±3 GHz (AMSU-B channels 17, 20, 19).

For the first channel triplet the assumption of equal emissivity is fulfilled because the three frequencies are so close to each other. For the second triplet, the same assumption is still used although the difference in frequencies is greater and some inaccuracy is introduced in the retrieval. In ~~the original paper (Miao, 1998)~~Miao (1998), it is argued that using this assumption for the second channel triplet represents a small error source when compared to other ones. Quantitatively it has been shown (Wang et al., 2001; Selbach, 2003; Selbach et al., 2003) that using the same emissivity assumption while including the 150 GHz channel will cause a positive bias of up to 0.5 kg/m^2 depending on the type of surface. We can simplify the expression of brightness temperature given in Eq. (1) by taking the difference of two brightness temperatures measured at two different channels i, j, so that we get

$$\Delta T_{ij} \equiv T_{b,i} - T_{b,j} = (T_0 - T_c)(1-\epsilon)(e^{-2\tau_j sec\theta} - e^{-2\tau_i sec\theta}) + b_{ij}. \quad (2)$$

~~Because the T_s term is the same for both brightness temperatures, it has disappeared from Eq. as a result of the subtraction.~~ To account for the differences in the m_p term, the bias term b_{ij} was introduced.

$$b_{ij} = T_s(m_{p,i} - m_{p,j}). \quad (3)$$

As shown in Melsheimer and Heygster (2008) - Appendix II, a good approximation for this term is

$$b_{ij} \approx \int_0^\infty [e^{-\tau_j(z,\infty)sec\theta} - e^{-\tau_i(z,\infty)sec\theta}] \frac{dT(z)}{dz} dz. \quad (4)$$

Here, $T(z)$ stands for the temperature profile of the atmosphere with height z. To find the relationship between the measured brightness temperature and the water vapour absorption that

does not depend on any other surface parameter we require the third brightness temperature measured in channel k. With this, a pair of brightness temperature differences is available from which the ratio will be

$$\eta_c \equiv \frac{\Delta T_{ij} - b_{ij}}{\Delta T_{jk} - b_{jk}} = \frac{e^{-2\tau_i sec\theta} - e^{-2\tau_j sec\theta}}{e^{-2\tau_j sec\theta} - e^{-2\tau_k sec\theta}}. \quad (5)$$

By using the two brightness temperature differences between three brightness temperatures and taking the ratio of these differences all terms that depend on surface parameters have been simplified and now we have a direct relationship between the measured brightness temperatures and atmospheric opacity due to water vapour absorption. Following the naming convention in Melsheimer and Heygster (2008), we call the left hand side of Eq. (5) the ratio of compensated brightness temperatures, η_c (containing the correction terms b_{ij} and b_{jk}). η_c is independent of any surface contribution, and only influenced by the atmospheric opacity terms $\tau_{(i,j,k)}$ at the three channel frequencies. These atmospheric opacity terms in turn are functions of the amount of absorption by water vapour and oxygen and can be expressed as

$$\tau_i = \kappa_{vapour,i} W + \tau_{oxygen,i}\,, \quad (6)$$

where $\kappa_{vapour,i}$ is the water vapour mass absorption coefficient at channel i, $\tau_{oxygen,i}$ represents the oxygen contribution to the atmospheric attenuation at channel i, and W is the water vapour load. For the band channels around the 183.31 GHz frequency, the contribution of water vapour to the absorption is much stronger than for oxygen so that the $\tau_{oxygen,i}$ term will be neglected henceforth.

The aim is to have a direct connection between the ratio of brightness temperature and the water vapour content W. Using the approximation introduced by Miao (1998), the difference of exponentials can be transformed into a product of a linear and an exponential function so that eventually we get

$$\eta_c = \exp[B_0 + B_1 W sec\theta + B_2 (W sec\theta)^2]. \quad (7)$$

Here B_0, B_1, and B_2 depend on the mass absorption coefficients k for the three channels and are called bias parameters. Compared to the first two terms under the exponent ~~,~~ the quadratic term ~~can be neglected~~ is negligible small so that the logarithm of Eq. (7) becomes

$$\log \eta_c = B_0 + B_1 W \sec\theta. \tag{8}$$

The final retrieval equation for water vapour content W is then

$$W \sec\theta = C_0 + C_1 \log \eta_c, \tag{9}$$

where $C_0 = -\frac{B_0}{B_1}$ and $C_1 = \frac{1}{B_1}$ characterizing the atmospheric attenuation at the channel frequencies used. ~~They~~ These calibration parameters are determined from simulated brightness temperatures ~~. As the atmospheric conditions vary throughout the globe, these simulations are run using~~ based on radiosonde profiles. The simulations were run using the ARTS (Atmospheric Radiative Transfer Simulator) ~~(Eriksson et al., 2011) for Arctic atmospheric profiles retrieved from radiosonde measurements.~~ radiative transfer model (Eriksson et al., 2011) which used as input radiosonde data collected from 29 coastal or island WMO (World Meteorological Organization) stations in the Arctic. The time period for the radiosonde measurements used is between 1996 and 2002.

By replacing the form of η_c from Eq. (7) in the ratio of brightness temperature differences from Eq. (5) we obtain the linear relationship between ΔT_{ij} and ΔT_{jk}

$$\Delta T_{ij}(\epsilon) = b_{ij} + \eta_c(W)(\Delta T_{jk}(\epsilon) - b_{jk}). \tag{10}$$

The brightness temperature differences depend on the surface emissivity ϵ while η_c only depends on W. In a ΔT_{ij} vs. ΔT_{jk} scatter plot with constant W and for varying ϵ, Eq. (10) describes a straight line of slope $\eta_c(W)$ that runs through the point (b_{ij}, b_{jk}). Because the two bias parameters vary only weakly with W and η, all lines obtained for different W values will cross or pass very near to one single point $F(F_{jk}, F_{ij})$, called focal point (Miao et al., 2001). To find its coordinates, brightness temperature simulations were run for eleven discrete values of ϵ. ~~For each simulation, realistic~~ As for the calibration parameters described above, the simulations

are run with the ARTS radiative transfer model using Arctic radiosonde profiles with realistic W ~~values are provided from radiosonde profiles of Arctic atmospheric conditions~~values as input. For all simulations, the surface temperature equals the ground level atmospheric temperature. For each constant W value, a line is fitted to the the points in the ΔT_{ij} vs. ΔT_{jk} scatter plot. The point of least square distance from all lines will be called the focal point F. By finding the focal point coordinates we have the relationship between the simulated brightness temperature differences and the W values and so fit Eq. (9), which allows us to determine the constant calibration parameters C_0 and C_1. With this method a total of four parameters, two focal point coordinates and two atmospheric calibration parameters are derived through the regression fit.

The principal problem with the ~~original~~ Antarctic algorithm was that the sensitive band channels around the 183.31 GHz frequency will reach saturation with relatively low amounts of atmospheric water vapour (Selbach, 2003). This means that after crossing a certain threshold value for W, the brightness temperature T_b does not vary with increasing W. Therefore, when one channel reaches saturation, it can no longer be used in the retrieval triplet for higher W values. For the first channel triplet (183.31 $\pm$7, 183.31$\pm$3, and 183.31$\pm$1 GHz), the first channel (AMSU-B channel 18 at 183.31$\pm$1 GHz) reaches saturation at 1.5 kg/m^2. To achieve a practical W retrieval range, the channel triplet (17, 20, 19, i.e. 150, 183.31 $\pm$ 7, and 183.31 $\pm$ 3 GHz) is used for values higher than 1.5 kg/m^2 and can function up to 7 kg/m^2 when channel 19 reaches saturation. As a practical test for when the algorithm should switch between the two channel triplets, the saturation point for a given channel k, as defined in Miao et al. (2001), is the W threshold value after which $T_{b,j} \leq T_{b,k}$, or simply

$$T_{b,j} - T_{b,k} \geq 0. \tag{11}$$

~~In the previous~~ This test is based on the threshold at which the brightness temperature of a given channel is no longer increasing with increasing W. This threshold represents the point at which the brightness temperature levels off and then starts to decrease again with increasing W. This happens as the signal that reaches the instrument no longer comes from the whole atmospheric column down to the ground but only from the colder, upper part of the atmosphere. In the original version of the Arctic algorithm (Melsheimer and Heygster, 2008), in order to extend the

retrieval range, the above condition has been relaxed. The saturation cut-off temperature, $T_{bj} - T_{b,k} \geq 0$ has been modified to $F_{20,19}$ ($T_{bj} - T_{b,k} \geq F_{20,19}$), with $F_{20,19}$ being a few Kelvins. This modification translates into an increase in the retrieval range by about 1 kg/m^2 at the expense of increased error as the channel approaches its saturation limit. If the difference $\Delta T_{jk} - F_{jk}$ is smaller than $-10\,K$ the corresponding error for the second channel triplet (17, 20, 19) is below 0.4 kg/m^2 for the retrieval range 1.5 – 7 kg/m^2. For the first channel triplet (20, 19, 18) which has the narrow retrieval range of 0 – 1.5 kg/m^2 the error is below 0.2 kg/m^2. This particular issue of the relaxed conditions will be addressed in the final algorithm (Section 2.7). These specific cases where the Melsheimer and Heygster (2008) algorithm would only retrieve data under the relaxed condition scenario were found to be mostly open water regions where the equal emissivity assumption failed. The new components that deal exclusively with retrieval over open water use the condition in Eq. (11).

2.3 Extending the TWV retrieval range

Normally, for TWV values above 7 kg/m^2, saturation occurs at channel 19 (183.3±3 GHz). To extend the retrieval range above this threshold, a new channel is necessary to take its place in the triplet, which means that a new set of assumptions has to be made about the surface emissivity influence. Now, the three channels i, j, k represent AMSU-B channels 16, 17 and 20 (89,150 and 183.31±7 GHz). Because channel 16 is so far apart from the other two, we can no longer assume that it has the same surface emissivity as the others. Therefore, we will have $\epsilon_i \neq \epsilon_j$ for the new channel i and $\epsilon_j = \epsilon_k$ is the approximation used as before.

If we consider that we have two channels with different surface emissivities, the brightness temperature difference becomes

$$\Delta T_{ij} \equiv T_{b,i} - T_{b,j}$$

$$\Delta T_{ij} = (T_0 - T_c)(r_j e^{-2\tau_j sec\theta} - r_i e^{-2\tau_i sec\theta}) + b_{ij}, \tag{12}$$

where r is the ground reflectivity $(1 - \epsilon)$, and b_{ij} is the same as in Eq. (4) because it does not depend on the surface emissivity ϵ. The corresponding compensated ratio of brightness

temperature differences is

$$\eta_c = \frac{\Delta T_{ij} - b_{ij}}{\Delta T_{jk} - b_{jk}} = \frac{r_i e^{-2\tau_i sec\theta} - r_j e^{-2\tau_j sec\theta}}{r_j(e^{-2\tau_j sec\theta} - e^{-2\tau_k sec\theta})}. \tag{13}$$

Rearranging terms to resemble the original form in Eq. (5) we get

$$\eta_c = \frac{r_i(e^{-2\tau_i sec\theta} - e^{-2\tau_j sec\theta})}{r_j(e^{-2\tau_j sec\theta} - e^{-2\tau_k sec\theta})} - \left(1 - \frac{r_i}{r_j}\right)\left(\frac{e^{-2\tau_j sec\theta}}{e^{-2\tau_j sec\theta} - e^{-2\tau_k sec\theta}}\right). \tag{14}$$

After approximating the difference in exponentials as before, the compensated ratio of brightness temperature differences becomes

$$\eta_c = \frac{r_i}{r_j}\exp[B_0 + B_1 W \sec\theta + B_2(W\sec\theta)^2] - \left(1 - \frac{r_i}{r_j}\right) C(\tau_j, \tau_k), \tag{15}$$

where

$$C(\tau_j, \tau_k) = \frac{e^{-2\tau_j \sec\theta}}{e^{-2\tau_j \sec\theta} - e^{-2\tau_k \sec\theta}}$$

is a slowly varying function that depends only on the atmospheric absorption factors. In order to obtain a simple linear relationship between the compensated brightness temperature difference and water vapour load W we rearrange the above equation into

$$\log \eta_c\prime = B_0 + B_1 W \sec\theta + B_2(W\sec\theta)^2. \tag{16}$$

The modified ratio $\eta_c\prime$ includes the terms depending on the reflectivities and the $C(\tau_j, \tau_k)$ function

$$\eta_c\prime = \frac{r_i}{r_j}[\eta_c + C(\tau_j, \tau_k)] - C(\tau_j, \tau_k) \tag{17}$$

The final retrieval equation for W is obtained after eliminating the negligible quadratic term

$$W\sec\theta = C_0 + C_1 \log \eta_c\prime. \tag{18}$$

The difference between $\eta_c\prime$ and η_c is that the former depends on the surface emissivity through the reflectivities ratio $\frac{r_i}{r_j}$ while the latter is surface independent. To enable retrieval using Eq. (18), more information is needed about the behaviour of the surface emissivities at 150 and 89 GHz. Direct information about the surface emissivity for every satellite footprint is not available so we need to parametrize the emissivity and obtain a constant reflectivity ratio that would only roughly depend on the surface type ~~(~~ocean/ice/ land~~)~~. Identifying the major surface types in the Arctic is another task that has to be integrated into the algorithm. ~~The~~ Because at the time no ocean surface emissivity information was readily available and a proof of concept was needed first over regions with low enough TWV, the Melsheimer and Heygster (2008) algorithm extension ~~is~~ was adapted only for sea ice surfaces. The ~~source for the information about surface emissivity~~ sea ice surface emissivity data was obtained from the Surface Emissivities in Polar Regions-Polar Experiment (SEPOR/POLEX measurement campaign in 2001).

This campaign used an aircraft-mounted instrument, the Microwave Airborne Radiometer Scanning System (MARSS), which possesses two microwave channels of frequencies similar to those required for the algorithm extension. For AMSU-B channel 16 at 89 GHz, there exists the MARSS channel 88.992 GHz, and for AMSU-B channel 20 at 150 GHz there exists a corresponding MARSS channel at 157.075 GHz. This difference of 7 GHz does not pose significant issues for the retrieval using the 150 GHz channel. The difference between measurements at 150 and 157 GHz is between $\pm$ 0.01 calculated from the in situ measurements (Selbach et al., 2003; Selbach, 2003), while the emissivity variability for the different ice types is greater than this difference. Because of this, the impact on the final retrieval is considered negligible.

To obtain the reflectivity ratio, the regression of ϵ_{89} as a function of ϵ_{150} was calculated

$$\epsilon_{89} = a + b\epsilon_{150}. \tag{19}$$

For the ratio of reflectivities to be constant it has to be independent of the variable emissivities. Because of this the regression was constrained so that ϵ_{89} $(\epsilon_{150} = 1) \approx 1$. The physical meaning of this is that the emissivity for the two channels cannot be greater than 1. Using the constraint above means that $a + b \approx 1$ and so the reflectivity ratio only depends on the regression relation-

ship coefficient b

$$\frac{r_{150}}{r_{89}} \approx \frac{1}{b}. \tag{20}$$

From the data points over sea ice, the following regression relationship was found by Melsheimer and emissivity at 89 and 150 GHz

$$\epsilon_{89} = 0.1809 + 0.8192 \cdot \epsilon_{150} \tag{21}$$

By replacing the coefficient b in Eq. (20) we have the reflectivity ratio

$$\frac{r_{150}}{r_{89}} = 1.22. \tag{22}$$

It is indicated by Melsheimer and Heygster (2008) that this is just a partial compensation for the contribution of surface emissivity. The SEPOR/POLEX measurements were made in the winter season and therefore do not take into account the melt processes that take place in summer which can significantly alter the emissivity behaviour of the surface (Tonboe et al., 2003). Because other resources on the subject are sparse this was the only option to include the effects of surface emissivity into TWV retrieval.

Besides the two parameters C_0 and C_1 that account for the atmospheric conditions in the Arctic, the modified ratio of compensated brightness temperatures $\eta_{c'}$ requires the $C(\tau_j, \tau_k)$ term that depends on the atmospheric opacities and thus, directly on TWV. If one studies the behaviour of $C(\tau_j, \tau_k)$ with increasing TWV for values above 7 kg/m^2 the function varies only a little, and it can be approximated by a constant. According to ~~(Melsheimer and Heygster, 2008)~~Melshe a variation in $C(\tau_j, \tau_k)$ between 1.0 and 1.2 will result in a change of C_0 and C_1 in the third significant digit. In total we have the two focal point coordinates, the atmospheric parameters C_0 and C_1, and the slowly varying function approximated by the constant $C(\tau_j, \tau_k) \approx 1.1$. The set of four parameters is determined through regression by using simulated brightness temperatures and atmospheric data from radiosonde profiles as described in Section 2.2.

The weakness of the extended algorithm is its sensitivity to changes in the reflectivity ratio. In other words, for sea ice surfaces where the surface emissivity deviates within the uncertainty

limits of $\sigma_{r_j/r_i} = 0.09$ (Melsheimer and Heygster, 2008) from the constant emissivities ratio used, the retrieval error can be as high as 3 kg/m^2.

Because of the specific channel triplet used by each sub-algorithm, the set of four calibration parameters has to be determined for the ~~L (low TWV), M (~~low TWV, mid-TWV ~~) and X (~~and extended-TWV ~~)~~ cases. In the new algorithm, two extra sets of calibration parameters are required, for the ~~M-ow (~~mid-TWV over open water ~~) and X-ow (~~and extended-TWV over open water ~~)~~ components.

2.4 Modifying the extended algorithm for use over open ocean

In Melsheimer and Heygster (2008) the possibility of using the same technique of incorporating surface emissivity information for the purpose of using the extended range component over open water regions in addition to sea ice-covered areas was considered as a possible improvement but was not investigated further.

In order to determine the feasibility of this option, a suitable linear relationship between surface emissivities at channels 150 and 89 GHz is required. By reusing the retrieval equation and replacing the calibration coefficients and the ratio of reflectivities, a separate module for retrieving water vapour in the extended range only over open water can be implemented.

The ocean emissivity model FASTEM (FAST surface Emissivity Model for microwave frequencies) takes into account the characteristics of the AMSU-B instrument, ~~and the~~ sea surface temperature and roughness (Hocking et al., 2011). The parameter that was found to determine a strong variation in surface emissivity is the ocean surface roughness. Surface roughness in turn is determined by wind speeds. At the typical range of values encountered in the Arctic (8–20 m/s), surface emissivity is determined mainly by wind speed. Figure 1 shows the behaviour of the ocean surface emissivities for the five channel frequencies of the AMSU-B instrument. Because the frequencies of the three band channels around 183.3 GHz are so close to each other, the corresponding emissivities are almost identical and thus represented by only one curve on the graph. Important to notice is the big difference between the curve for 89 GHz and the one for 150 GHz, which illustrates why the assumption of equal emissivities cannot be sustained for these pairs of channels. Also the difference between the 183.3 GHz and the 150 GHz curves that

is neglected by using the assumption of equal surface emissivity for the medium TWV retrieval range must be noted.

2.5 Ocean surface emissivity for the extended range 89,150,183.3±7 GHz triplet setup

Following the same method as for the extension over sea ice, through a linear regression between the ocean surface emissivity at 150 and at 89 GHz (panel a) of Fig. 2) we found the following linear relationship in the form of (10)

$$\epsilon_{89} = 1.2698 \cdot \epsilon_{150} - 0.2687. \tag{19}$$

For the emissivity of sea ice, studied for the first retrieval range extension, the constraint $\epsilon_{89}(\epsilon_{150} = 1) \approx 1$ had to be imposed on the system in order to express the ratio of reflectivities as a constant of the form shown in Eq. (7) independent of variable surface emissivity. Following the same logic, from the linear expression above we got the ratio of reflectivities

$$\frac{r_{150}}{r_{89}} = 0.7875.$$

Using this relationship, the calibration parameters C_0 and C_1 were also determined from regression between ~~atmospheric water vapour content~~ W from radiosonde profiles and simulated brightness temperatures as described in Section 2.2.

2.6 Ocean surface emissivity for the mid range 150, 183.3±7, and 183.3±3 GHz triplet setup

One of the error sources in the original algorithm was the assumption of equal surface emissivity for the 150 GHz and the 183.3 GHz band channels. Over open ocean, the differences in surface emissivity at these frequencies can lead to a positive bias in the TWV retrieval. Following the same methodology as for the lowermost channel triplet (89, 150, 183.3±7 GHz), a linear relationship can be retrieved from simulated ocean surface emissivity data for the frequency

triplet (150, 183.3±3, 183.3±7 GHz). From this, a reflectivity ratio can be obtained and used in a modified retrieval equation. This modification leads to an improvement in the bias when retrieving in the TWV range 2-6 kg/m^2 over ice-free ocean surfaces.

Following the regression fit in ~~Fig. panel b)~~ Figure 2 we obtained the linear relationship for ocean surface emissivity at 150 and 183 GHz

$$\epsilon_{150} = 1.1022 \cdot \epsilon_{183} - 0.1028 \tag{24}$$

from which we obtain the ratio of reflectivities as

$$\frac{r_{183}}{r_{150}} = 0.9073.$$

In addition to the C_0 and C_1 parameters, the $C(\tau_j, \tau_k)$ function that depends on the atmospheric opacity is necessary for a retrieval when a different surface emissivity is considered (Section 2.3). This function depends directly on TWV and it has been shown that above 7 kg/m^2 it is constant for the 89 and 150 GHz frequencies. ~~In the process of modifying the mid-TWV algorithm, the $C(\tau_j, \tau_k)$ was recalculated for the 183±7 and the 150 GHz channels and set as a constant $C(\tau_j, \tau_k) \approx 1.15$ in the retrieval Eq. .~~

For the ~~mid-TWV~~ channels used in the mid-TWV range retrieval module, the function $C(\tau_j, \tau_k)$ behaves differently than for the extended-TWV channels. Between 2 and 6 kg/m^2 it drops rapidly from 1.4 down to 1.0 (Fig. 3), but it has been found (Melsheimer and Heygster, 2008) that changes on the order of 0.2 in $C(\tau_j, \tau_k)$ lead to differences in the third significant digit of the C_0 and C_1 parameters, which is small compared to other error contributions. In the process of modifying the mid-TWV algorithm, the $C(\tau_j, \tau_k)$ was recalculated for the 183±7 and the 150 GHz channels and set as a constant $C(\tau_j, \tau_k) \approx 1.15$ in the retrieval Eq. (18).

2.7 ~~Arctic~~ TWV algorithm synthesis

The final structure of the new algorithm comprises a collection of independent retrieval modules, each tuned to a different set of surface and atmospheric parameters. This structure can be viewed in Table 1 where the SSM/T2 Antarctic algorithm by Miao et al. (2001), the original

AMSU-B Arctic retrieval algorithm by Melsheimer and Heygster (2008) and the new AMSU-B algorithm are described. The main modules represent the three different channel triplets, low, mid and high, that are used in the different retrieval ranges of TWV. Further differentiation into sub-modules is made by distinguishing between sea ice or open water, leading to five modules in total. One of the main differences between the new and the original AMSU-B algorithm is the use of the emissivity relationship in equation 19 for applying the extended-TWV retrieval over open water areas. This allows for retrieval over a greater spatial domain as the original algorithm could only use the mid-TWV sub-algorithm over open water for TWV values up to 7 kg/m^2.

The other addition over the original AMSU-B algorithm is that the mid-TWV sub-algorithm differentiates between sea ice/land and open water and has different retrieval equations for each of the two cases. We believe that this is a more physically consistent treatment than using the equal emissivity assumption. The specific open water module uses the regression relationship in equation 24, while the sea ice/land module uses the equal emissivity assumption. In the original algorithm mid-TWV retrieval over open water also operates under the equal emissivity assumption.

The algorithm for low-TWV uses AMSU-B channels 20, 19, and 18 for the retrieval range 0 to 1.5 kg/m^2. These are the band channels around the strong water vapour line at 183.31 GHz, and have the best accuracy and present the lowest error as the assumption of equal surface emissivity is valid for these three frequencies.

The mid-TWV algorithm using AMSU-B channels 17, 20, and 19 takes over retrieval up to 7 kg/m^2. It is assumed to be independent of the surface type but the retrieval error might increase when approaching the upper retrieval limit. The assumption of equal emissivity is still used over sea ice covered surfaces, even though there are some differences because of the introduction of the 150 GHz channel instead of the 183$\pm$1GHz channel. Because of this difference in real surface emissivity a positive bias of up to 0.5 kg/m^2 is possible (Selbach, 2003). Over areas with ~~lower~~ sea ice concentration ~~(~~below 80% SIC ~~) the speciffic~~ the specific open water sub-module of the mid-TWV algorithm uses the ratio of reflectivities at 183 and 150 GHz ~~is used~~ in order to account for the different surface emissivities of open water at these frequencies.

The extended-TWV ~~algorithm~~ module uses the channels ~~16~~20, 17, and ~~20~~ 16 to retrieve TWV in the range 7 - 15 kg/m^2. Previously, the retrieval from these channels was restricted to sea ice regions and because of the simplified treatment of the surface emissivity difference, the error ~~may~~ can reach 3 kg/m^2. Similarly with the mid-TWV module above, a dedicated open water ~~sub-module~~ version of the extended-TWV ~~algorithm~~ module uses the ratio of reflectivities at 89 and 150 GHz over scenes with mixed water and sea ice (the).

Due to of the specific channel triplet used by each ~~sub-algorithm~~sub-module, the set of four calibration parameters has to be determined for the ~~L (low TWV), M~~ (low TWV, mid-TWV ~~) and X (~~and extended-TWV ~~)~~ cases, and two extra sets for the new ~~M-ow and X-ow~~ mid and extended-TWV retrieval scenarios over open water.

2.8 How the retrieval works

One of the critical points in ~~the algorithm was~~ all of the AMSU-B algorithms is to correctly identify when one certain triplet of channels ~~would become~~ becomes saturated in order to switch to the next available triplet. In the ~~original~~ initial Antarctic algorithm paper by (Miao et al., 2001), this was accomplished by checking the sign of the brightness temperature difference using the condition in Eq. (11).

In order to extend the coverage while keeping the retrieval error reasonably low, the constraint above was relaxed in (Melsheimer and Heygster, 2008) by allowing the brightness temperature difference to go slightly above zero so that in the end, the following condition is applied:

$$T_{b,j} - T_{b,i} < F_{i,j}. \tag{26}$$

$F_{i,j}$ is the focal point calculated for a particular channel triplet. It usually has a value of a few Kelvin. The retrieval will work as long as the sign of the brightness temperature differences ratio η_c is positive.

This relaxed condition allows the channel triplet to be used until its high absorption channel approaches saturation and allows an extension of the retrieval range of that triplet by up to

1 kg/m^2. The disadvantage of this relaxed condition is that the retrieval error also increases when a channel in the triplet is close to saturation.

By mapping (not shown) the pixels according to the conditions used in their retrieval with the original algorithm we found that the values near the saturation limit retrieved under the relaxed conditions in most cases account for open water or mixed water/sea ice surfaces. This is where the equal emissivity assumption breaks down because the microwave emissivity of water is much lower than that of sea ice producing an increased retrieval error. In this new algorithm we propose to use a specific method for those areas.

For the mid and extended TWV range algorithms there is a further differentiation in the modules used between sea ice and open water surfaces. Based on our experience, a threshold of 80% sea ice concentration was chosen in order to differentiate the typically dry areas of high sea ice concentration in the central Arctic and the regions with a larger ratio of open water to sea ice where higher atmospheric water vapour loads are expected. In these peripheric regions the new algorithm is employed. In all areas with sea ice concentration above 80% the retrieval technique from ~~Melsheimer and Heygster(2008)~~ Melsheimer and Heygster (2008) is used, which is better suited for the very low atmospheric water vapour values encountered in this region.

To illustrate how the new algorithm works with these new sets of conditions we will present each step, with its differences to the previous method.

1) The algorithm begins by using the full set of five brightness temperatures of the AMSU-B instrument. In the previous method, it would first identify pixels where the conditions

$$T_{b,19} - T_{b,18} < F^L_{19,18} \text{ and } T_{b,20} - T_{b,19} < F^L_{20,19}$$

hold true. Here $F^L_{19,18}$ and $F^L_{20,19}$ are the pairwise focal points for channel pairs (18,19) and (19,20). This condition fulfilled allows for the channel triplet (18,19,20) to be used for the range up to 2 kg/m^2. Because the retrieval range of the first two channel triplets (low and mid range) overlaps around 2 kg/m^2 we will keep the stricter condition from the ~~original algorithm (Miao et al., 2001)~~Antarctic algorithm (Miao et al., 2001).

$$T_{b,19} - T_{b,18} < 0,\ T_{b,20} - T_{b,19} < 0.$$

For these pixels the low-TWV algorithm is applied.

2) If the first condition fails, the second one is checked. In the previous method this was

$$T_{b,20} - T_{b,19} < F^{M}_{20,19} \text{ and } T_{b,17} - T_{b,20} < F^{M}_{17,20}.$$

Continuing from the strict zero threshold condition for the low-TWV, the new condition threshold is

2a) $T_{b,19} - T_{b,18} \geq 0$ and $T_{b,20} - T_{b,19} < 0$ and $T_{b,17} - T_{b,20} < 0$.

This test is performed for pixels with over 80% sea ice concentration. Where this is true, the ~~classical~~ original mid-TWV retrieval is used.

2b) Over open water and scenes with ice concentration below 80% in the mid TWV range, the algorithm now uses a somewhat different condition

$$T_{b,19} - T_{b,18} \geq 0 \text{ and } T_{b,20} - T_{b,19} < F^{X}_{20,19} \text{ and } T_{b,17} - T_{b,20} < F^{X}_{17,20}$$

Condition 2b) means that the pixels which were previously retrieved under the equal emissivity assumption over open water will now be treated separately according to their surface type taking into account the surface emissivity component. Those pixels that are at the saturation limit for the mid range, but do not contain open water are being flagged for further processing with the extended range sea ice algorithm. This would include pixels retrieved above land in less dry conditions (in the Arctic case this means TWV $> 2\,\mathrm{kg/m^2}$).

3) For applying the extended-TWV algorithm, the remaining pixels are tested for

$$T_{b,17} - T_{b,20} < F^X_{17,20} \text{ and } T_{b,16} - T_{b,17} < F^X_{16,17},$$

and where true, processed. In addition to this test for channel saturation, the data is again classified for its surface type, and only sea ice or open ocean areas are kept excluding land. This surface classification is done for all channels by a comparison with sea ice concentration maps derived ~~from SSMIS~~ using the ARTIST Sea Ice concentration retrieval (**?**) from SSMIS (Special Sensor Microwave Imager / Sounder) or AMSR-E (Advanced Microwave Scanning Radiometer - Earth Observing System) data depending on the retrieval date.

2.9 ~~Comparison of results with~~ Comparing the ~~previous method~~new retrieval with other TWV retrieval products

For a comparison we use daily averages for thirty consecutive days in each of four months, September, March, June and December which represent the variability of the atmospheric parameters and sea ice extent. September and March represent the two extremes of sea ice extent. The minimum extent in September is usually coupled to warmer air and higher atmospheric water vapour load. The maximum extent in March corresponds to lower air temperatures and a drier atmosphere. June and December represent transition periods between the two extremes.

In order to obtain a bigger data sample we ran this analysis using daily averaged data for three consecutive years from 2007 to 2009. The geographical domain we chose represents the entire Northern Hemisphere above 50° N latitude. Though the very first retrieval was targeted towards the Central Arctic region, this was because the atmospheric water vapor load over this region was low enough for the algorithm to retrieve. After the subsequent extensions of the retrievable TWV range, the geographical domain for applying the algorithm has increased as well. For the purpose of this work we have arbitrarily chosen this 50° N limit because that is the approximate latitude where the water vapor load in winter is low enough to allow for a time consistent retrieval with the newest version of the algorithm. All ~~landmases~~ landmasses in this region are also included because the method is able to retrieve TWV there if the values are low enough. For example Greenland is always included in the retrieval because the atmosphere above it is dry throughout the year.

From AMSU-B data we produce two versions of the TWV product, one retrieved with the original Melsheimer and Heygster (2008) method and the other with the new algorithm. The calibration parameters we derived separately for each channel combination with the corresponding linear relationships between surface emissivities from the same batch of radiosonde TWV data.

First we want to see how the new retrieval method performs against the original one and hence test both methods against two other TWV products chosen as benchmarks in this field. The first benchmark is the ECMWF (European Center for Medium Range Weather Forecasts) ERA-Interim (?) reanalysis model data from which TWV values were derived.

The second dataset is the TWV product from Remote Sensing Systems (RSS) that uses AMSR-E brightness temperatures and an algorithm adapted from (Wentz, 1997). This retrieval algorithm has been developed for global coverage and works over all ice free ocean surfaces. Because of this it can cover a large range of TWV values (0 - 75 kg/m^2) but it was not specifically tuned for the dry Arctic conditions. This data set covers the entire nine year lifespan of AMSR-E and has been used for creating derived products (Smith et al., 2013) and validated against ship based observations (Szczodrak et al., 2006) and hence is considered a good benchmark against which the new AMSU-B retrieval can be compared.

A third test dataset was obtained from the ~~Bobylev et al. (2010)~~ (Bobylev et al., 2010) algorithm. This method is a neural network based approach designed specifically for the ice free regions in the Arctic. As a training dataset for the neural network the authors used radiosonde data from Russian polar stations. The method is able to retrieve low TWV values over open ocean areas using the same AMSR-E instrument as the RSS TWV product with similar TWV value ranges. This neural network approach is proven to have a smaller root mean square error than the Wentz global algorithm used in the RSS TWV product. These three retrievals are compared over one common valid spatial domain (only open water) while using the ECMWF TWV data as a reference point.

3 Results and Discussion

3.1 ~~Original versus new AMSU-B retrieval~~Comparison of results to Melsheimer and Heygster (

Independent of the comparison benchmark, an important difference between the original and the new retrieval is the area the algorithm can cover for retrieving TWV in the Arctic~~region~~. Because both algorithms use the same instrumental input, a one to one comparison of coverage represented as the number of valid retrievable pixels is possible.

~~Figure ?? shows the difference in coverage~~

Figure 4 shows two examples in the coverage difference between the original and the ~~improved AMSU-B algorithm. Large features can be recognized consistently, such as the drier air masses over Greenland, around the North Pole and in northern Canada. It can be argued that having good temporal and spatial coverage using a satellite retrieval albeit with reduced accuracy is preferable to high accuracy field measurements of local coverage and limited temporal resolution.~~

new retrieval, for one summer and one winter day. The largest benefit of the new retrieval is that large areas in the North Atlantic and Pacific oceans can now be covered. The only limitation of the method is the amount of water vapor present in the atmosphere and, for the extended range module, the presence of either an open water or sea ice covered surface. In both the summer and winter case the new method has a larger coverage area, with the biggest difference being seen in the summer case. To add to this analysis, Figure 5 presents the frequency of retrieval for the new and the original retrieval versions when looking at the months of June and December for the whole three year interval studied. Each pixel value represents the number of times that particular region has been present in the daily retrieval maps for the test time series. The minimum value shown is five while the maximum is 90 days. As in the one day example of Figure 4, the increase in coverage for the month of June is evident, with the addition of North Atlantic and Pacific Ocean regions where the water vapor values are within the retrieval range. For December the frequency of retrieval has been improved where these same ocean regions can now be retrieved more consistently with the new algorithm.

When comparing the two AMSU-B retrieval methods for the whole testing time series we look at monthly averages compiled from swath data for each method. The comparison was done for the representative four months of each year from 2007 to 2009 in order to see how the total area of retrievable pixels is affected by the new method (Fig. 6). In the colder months of March and December the benefit of the new method is marginal because of the larger sea ice extent (when compared to the summer months) and the overall low water vapour burden of the atmosphere. In these months we can observe a small increase of 17.4% and 21.18% respectively, compared to the coverage of the original algorithm. For September and June the number of retrievable pixels increase by 152% and 176%, respectively of the original number (Fig. 6). This change is significant considering that these areas were beyond the retrieval capabilities of the ~~previous~~ original method.

ECMWF ERA-Interim reanalysis data was used as reference in order to compare the original method and the new one. The ECMWF TWV information was directly compared to collocated daily averages from both algorithms. In terms of correlation with the ECMWF, the two algorithms vary significantly (Fig. ~~??~~7).

The new method matches the correlation of the original one for the month of March (0.86), and even surpasses it for December (0.82 vs 0.77). In the months with moist conditions and lower sea ice extent, June and September, the correlation drops to 0.36 and 0.32 vs 0.57 and 0.61, respectively. Comparing this with the results in Fig. 6 shows that in the months where the spatial contribution of the improved algorithm is greater, the correlation drop is more significant. ~~Most of this contribution represents pixels with large TWV values , close to the retrieval limit that have a higher uncertainty .~~ For a more detailed look into the differences between the original and new AMSU-B methods a side by side comparison is presented in Figure 8. Here the original and new algorithm are compared with each other and then individually with ECMWF TWV over the same common domain valid for both retrievals. One major difference between the two algorithms is in the way mid-TWV retrieval is performed. The new algorithm uses a dedicated open water sub-module while the original algorithm treats all surface types the same in this retrieval range. While the small differences in calibration parameters can cause minor differences in the low-TWV domain where the retrieval equations are identical, the different

treatment of the surface type causes a larger deviation between the results at the upper limit of the mid-TWV range. Another modification that has an impact on the new retrieval are the differences in trigger thresholds which cause the algorithm to switch to a different retrieval module. These thresholds and the differences between the new and original versions have been described in Section 2.9. Because of the stricter switching condition, the new algorithm switches to the extended range retrieval module earlier than the original algorithm and retrieves higher TWV values. These data points which are retrieved with the extended range module in the new version and with the mid-TWV module in the original one can be seen as a plume of higher AMSU-B new TWV values which deviate from the identity line in the left side plot of Figure 8. The comparison of the new algorithm with ECMWF TWV in the right most plot of the same figure indeed shows a similar cloud of overestimated data points closer to the maximum retrieval limit of the algorithm.

From Figure 9 where the new algorithm is compared against ECMWF TWV over its full spatial domain of valid retrievals the higher uncertainty of data points with larger TWV value is evident. The scatter in the retrieved data increases with the retrieved TWV value. When the retrieved values approach 15 kg/m^2 the involved channels are near the saturation limit so that the true value may well exceed this retrieval limit. As a practice for future studies we recommend to only use retrieval values up to 14 kg/m^2. It is however important to note that the majority of data points retrieved fall within the 0-6 kg/m^2 interval which matches well with the model data. The extended range retrieval represents the maximum coverage that can be obtained with this instrument and algorithm combination. This increased coverage with the price of increased uncertainty represents the only way to consistently cover regions where a complete data gap existed before in mixed sea ice/open water regions. In these areas other retrieval methods, like the AMSR-E based ones presented in Section 2.9, cannot function because of the presence of sea ice while the original AMSU-B algorithm could not retrieve anything because of the presence of open water and high TWV values.

When considering the difference between the ECMWF data and the AMSU-B retrieval, the highest bias is again seen in the warmer months (Fig. 10).

~~In the month of March the bias~~ Following the correlation results shown in Figure 7, the higher variability of the new ~~method has dropped by almost half to −0.27 from −0.43 kg/m^2 in the original retrieval. For December there is an increase from −0.06 to −0.3~~AMSU-B retrieval is confirmed by the root mean square difference against ECMWF data which are represented by the error bars in Figure 10. The bias behaviour versus ECMWF has changed from the original to the new algorithm. Both retrievals follow the same pattern of low bias in winter and higher bias in summer months. This can be explained by seasonal variability in the mean water vapor load of the atmosphere. In winter months the mean ECMWF TWV is usually below 8 kg/m^2 ~~. The most interesting change comes for June and September, where there is an increase of the bias as well as a change of sign. Earlier the algorithm was underestimating in both months compared to ECMWF by −0.38~~ which represents the lower range of possible retrieval for the mid-TWV module. In summer months this average value is between 13 and ~~−1.94 respectively and now we register an overestimation of TWV by 1.86 and 1.29~~15 kg/m^2 ~~, respectively. Thus, the increase of bias becomes highest in June~~which sits in the upper range of the extended TWV module, the module most susceptible to higher uncertainties. The change in winter months is an improvement over the original, with the bias versus ECMWF decreasing throughout the winter months. For the winter months the new method registers an increase in bias when compared to the original in the month of June for 2007 and 2008, while scoring a lower value in 2009. These differences are small however and we prefer to focus on the seasonal variability which is matched between the two algorithm versions with one notable exception. While similar in absolute value, the new method bias in the month of September for each of the three years shows a sign inversion when compared to the original method. When the latter was on average underestimating TWV against ECMWF data, the new algorithm shows an overestimation for the same months. Considering the technical differences between the two algorithms, this change in behaviour can be attributed to the split of the extended algorithm in sea ice and open water sub-modules respectively. The open water extended range module of the new algorithm returns overestimated TWV values when compared to collocated ECMWF data. This confirms the behaviour observed in Figure 8 where when compared over the same domain, the new algorithm extended TWV module seems to overestimate the retrieval when compared

to model data. Another agreement on the behaviour of the new algorithm retrieval can be seen between Figures 8 and 10 where the large variability of the new algorithm retrieval at higher TWV values is evident.

3.2 Intercomparison of New AMSU-B retrieval, RSS TWV and Neural Network method

With this comparison we ~~wanted to see how~~ explore how well the new AMSU-B retrieval matches other retrieval methods like the RSS TWV product and the retrieval based on the neural network approach. As a benchmark data set we chose the ECMWF TWV data. Even though circulation model data in general does not represent a source for validating satellite retrieval products, it may serve as a consistent data set from which the retrievals should not deviate too much. While a match between the model data and any one retrieval does not represent validation, any large deviations from the model could signify errors in the retrieval data. We expect to conclude whether or not the output of the new AMSU-B algorithm is reasonable and warrants further development and validation efforts.

To judge if a ~~method specific bias exists~~ method-specific bias exists versus the model and if a seasonal variability is present, monthly differences were calculated between the ECMWF data and each retrieval using daily averages. ~~In Fig.~~ To allow an intercomparison between them all retrieval products plus the ECMWF model data are gridded to one common grid so that the spatial domain used in the comparison always represents the largest common domain for all represented data sources. In Figure 11 the individual monthly bias values are shown for each of the three methods over open ocean areas above 50° N. The method specific bias as well as the ECMWF mean value was calculated for the same domain common to all methods.

Two of the retrievals compared here show a seasonal variation in bias. Both the AMSR-E based neural network and the AMSU-B retrieval underestimate TWV when compared to the model with the former showing the lowest bias throughout the entire dataset. The AMSR-E RSS retrieval presents a ~~constant overestimation~~ small constant overestimation of around 1 kg/m^2 throughout the entire dataset without any strong seasonal characteristics. This behaviour of the RSS product matches the findings of (Bobylev et al., 2010) where it is shown that the global Wentz retrieval tends to overestimate water vapour content in the dry conditions of the Arctic.

The AMSU-B retrieval shows good results in winter when its low bias values place it close to the neural network retrieval with performance comparable to the RSS retrieval. ~~While the~~ The AMSU-B method shows much higher negative bias values in summer~~it is important to note that~~ . Then, the average TWV values for the ice-free ocean ~~in the summer months~~ frequently surpass the saturation value of 15 kg/m^2, so that the AMSU-B retrieval works at the limits of the algorithm where the higher uncertainty is assumed.

Figure 12 top displays the average TWV value of each retrieval method ~~for the entire ice-free Arctic Ocean~~calculated over the same domain as in Figure 11. The results of the neural network method closely ~~follows~~ follow the model value throughout the year. The new AMSU-B retrieval matches the model almost as well in the winter months while ~~summer months~~ in the summer months it present a more pronounced underestimation with respect to the ECMWF TWV average values.

Because the intercomparison with the two AMSR-E based methods can only be done for ice-free ocean areas, the assessment of the new AMSU-B retrieval cannot be complete without taking into account the strong points of this approach, which is that it can retrieve TWV over the entire Arctic scene including land and sea ice-covered as well as open ocean surfaces. To this end a final comparison is made for ~~the~~ average TWV over the ~~Arctic for the complete retrieval area~~ whole valid domain of the new AMSU-B ~~method. This is shown in Fig.12 bottom and the~~ retrieval (Fig. 12 bottom). The performance increase throughout the year is obvious when compared to the open ocean regions alone. The average retrieved TWV for winter months matches better with the model while the overestimation for summer months, although still present is greatly diminished. Also important to note is how much the average ECMWF TWV value decreases in the summer months (from 15 kg/m^2 to 10.5 kg/m^2 in June and from 12.8 kg/m^2 to 11.9 kg/m^2 in September) once the ice-covered regions of the Central Arctic are added to the comparison. This shows the difference between the average atmospheric water vapour load ~~in the dry Central Arctic compared to the~~ for the entire Arctic when including all sea and land ice covered regions and the higher TWV ice-free Arctic Ocean~~areas~~.

4 Conclusions

Based on the previous work of ~~Miao et al. (2001) and Melsheimer and Heygster (2008)~~(Miao et al., 200 Melsheimer and Heygster (2008), we present a method to achieve a more complete coverage for TWV retrieval in the Arctic region. The previous method was able to retrieve TWV over all surface types for atmospheric water vapour loads up to ~~6~~7 kg/m^2 and over sea ice for up to ~~15~~14 kg/m^2. The new method extends the coverage of the maximum range retrieval over open water where higher values for TWV are frequently found, especially in summer when the sea ice extent is small. This aspect has become even more important in the last decade with the dramatically decaying Arctic summer sea ice~~extent~~.

Because of the unique way in which each of the three cases of channel coupling and surface types are handled, the algorithm has become more complex. Each of the five sub-algorithms ~~are~~ is designed with a set of specifically derived calibration parameters and three of them (Mid TWV range-open water, extended TWV range, extended TWV range-open water) use retrieval equations that take into account a linear regression between the surface emissivity at 89 and 150 GHz.

The modifications brought to the AMSU-B retrieval are meant to improve the retrieval over mixed areas of sea ice and open water by including a comprehensive treatment of the open ocean emissivity. Another ~~expected~~ improvement is the increase in retrievable area ~~to the maximum extent possible by assuming the algorithm saturation limit of 15 kg/m^2.~~ under the condition of a recommended upper limit of 14 kg/m^2 for valid values.

The new method shows an improvement both in correlation (Fig. ~~??~~7) and bias (Fig. 10) with ECMWF data for the winter months, and a large increase in coverage for the summer months (~~Fig. 12,Fig. ??~~Figs. 4, 5, 12) because of the dedicated treatment of open water emissivity in the mid and high TWV ranges. When compared to ECMWF reanalysis data, the new algorithm is shown in Fig. 10 to have a higher ~~RMS difference~~ RMSD than the original one, with average ranges from 1.86 kg/m^2 (1.08 kg/m^2 previously) in March, up to 5.67 kg/m^2 (3.79 kg/m^2 for the original algorithm) in September. This difference can be explained by the additional area covered with the new algorithm which adds high TWV value and high uncertainty data points

to the comparison. This can also be seen from the 2D histograms in Figures 8 and 9. For the month of September we have an increase in average coverage of ~~176~~174% as compared to 17,4% for March (Fig. 6). This accounts for all of the open ocean areas where the extended range sub-algorithm can now be employed with the connected higher error margins previously acknowledged in ~~Melsheimer and Heygster (2008)~~Melsheimer and Heygster (2008).

When comparing the new method with two established algorithms for retrieving atmospheric water vapour over open ocean it is shown that the new AMSU-B retrieval method has similar performance in winter months (Figs. 10, 11). As these two AMSR-E based methods are restricted to open water areas where the atmospheric water vapour load is higher in the summer months, the AMSU-B algorithm performance decreases correspondingly in these conditions because of the relatively low saturation limit of 15 kg/m^2. The neural network approach by ~~Bobylev et al. (2010)~~ (Bobylev et al., 2010) ranks first as the most accurate retrieval when compared to ECMWF model data over open water only. The new AMSU-B method scores similarly in winter months while the RSS TWV product based on Wentz (1997) which was calibrated for global operation ~~displayed~~ displays a low but constant positive bias throughout the seasonal cycle. It is important to note however that the strength of new AMSU-B method is that it can seamlessly retrieve atmospheric water vapor loads over a large spatial domain which includes land and sea ice besides the open ocean areas where the established retrieval products have already proven themselves. The accuracy of the new AMSU-B retrieval relative to ECMWF data increases when the entire Arctic region is taken into account, including all sea and land ice areas. This demonstrates the capabilities of the method to retrieve TWV simultaneously over all surface types in the ~~dry~~ specific atmospheric conditions of the Arctic and adjacent regions. The new algorithm extends the spatial coverage in the warmer months where higher TWV values can be retrieved over open water and mixed surface regions. Data gaps present in the original method results are covered for the winter months as well. These high TWV measurements however are also connected with larger uncertainties as the algorithm is working near the limits of the instrument sensitivity.This approach requires a trade-off between achieving a high spatial coverage of the ~~Arctic area, while assuming~~ polar region, while accepting the lower accuracy

dictated by instrument limitations, or using multiple instruments/methods each with their inherent collocation and accuracy issues to cover the same region.

References

Bobylev, L. P., Zabolotskikh, E. V., Mitnik, L. M., and Mitnik, M. L.: Atmospheric Water vapour and Cloud Liquid Water Retrieval over the Arctic Ocean Using Satellite Passive Microwave Sensing, IEEE Trans. Geosci. Remote Sensing, 48, 283–294, doi:10.1109/TGRS.2009.2028018, 2010.

Das, S., Majumder, S., Chakraborty, R., and Maitra, A.: Simplistic approach for water vapour sensing using a standalone global positioning system receiver, Radar, Sonar and Navigation, IET, 8, 845 – 852, doi:10.1049/iet-rsn.2013.0312, 2014.

Dee, D. P., Uppala, S., Simmons, A., Berrisford, P., Poli, P., Kobayashi, S., Andrae, U., Balmaseda, M., Balsamo, G., Bauer, P., et al.: The ERA-Interim reanalysis: Configuration and performance of the data assimilation system, Quarterly Journal of the royal meteorological society, 137, 553–597, 2011.

Eriksson, P., Buehler, S. A., Davis, C. P., Emde, C., and Lemke, O.: ARTS, the atmospheric radiative transfer simulator, Version 2, J. Quant. Spectrosc. Radiat. Transfer, doi:10.1016/j.jqsrt.2011.03.001, 2011.

Held, I. M. and Soden, B. J.: Water vapour feedback and global warming, Annu. Rev. Energy Environ., 25, 441–475, 2000.

Hewison, T. J. and English, S. J.: Airborne retrievals of snow and ice surface emissivity at millimeter wavelengths, IEEE Trans. Geosci. Remote Sens., 37, 1871–1879, 1999.

Hocking, J., Rayer, P., Saunders, R., Matricardi, M., and Brunel, P.: RTTOV v10 Users' guide v1.5, http://research.metoffice.gov.uk/research/interproj/nwpsaf/rtm/docs_rttov10/users_guide_10_v1.5.pdf, 2011.

Hurst, D. F., Oltmans, S. J., Vömel, H., Rosenlof, V. H., Davis, S. M., Ray, A. E., Hall, E. G., and Jordan, A. F.: Stratospheric water vapour trends over Boulder, Colorado Analysis of the 30 year Boulder record, J. Geophys. Res., 116, doi:10.1029/2010JD015065, 2011.

Le, T. V. and Gallus Jr, W. A.: Effect of an extratropical mesoscale convective system on water vapour transport in the upper troposphere/lower stratosphere A modeling study, J. Geophys. Res., 117, doi:10.1029/2011JD016685, 2012.

Melsheimer, C. and Heygster, G.: Improved Retrieval of Total Water vapour Over Polar regions From AMSU-B Microwave Radiometer Data, IEEE Trans. Geosci. Remote Sensing, 46, 2307–2322, 2008.

Miao, J.: Retrieval of atmospheric water vapour content in polar regions using space-borne microwave radiometry, Alfred-Wegener Inst. Polar Marine Res., 1998.

Miao, J., Künzi, K. F., Heygster, G., Lachlan-Cope, T. A., and Turner, J.: Atmospheric water vapour over Antarctica derived from SSM/T2 data, J. Geophys. Res., 106, 10 187–10 203, 2001.

Selbach, N.: Determination of total water vapour and surface emissivity of sea ice at 89 GHz, 157 GHz and 183 GHz in the arctic winter, Berichte aus dem Institut fur Umweltphysik, 21, 2003.

Selbach, N., Hewison, T. J., Heygster, G., Miao, J., McGrath, A. J., and Taylor, J.: Validation of total water vapour retrieval with an airborne millimeter wave radiometer over arctic sea ice, Radio Sci., 38, 8061, 2003.

Serreze, M. C. and Hurst, C. M.: Representation of mean Arctic precipitation from NCEP-NCAR and ERA reanalysis, Journal of Climate, 13(1), 182–201, 2000.

Smith, D. K., Mears, C., Hilburn, K. A., and Ricciardulli, L.: A 25-year satellite microwave mean total precipitable water data set for use in climate study, EUMETSAT Meteorological Satellite Conference, 2013.

Solomon, S., Rosenlof, K. H., Portmann, R. W., Daniel, J. S., Davis, S. M., Sanford, T. J., and Plattner, G. K.: Contributions of Stratospheric Water vapour to Decadal Changes in the Rate of Global Warming, Science, pp. 1219–1223, doi:10.1126/science.1182488, 2010.

Spreen, G., Kaleschke, L., and Heygster, G.: Sea ice remote sensing using AMSR-E 89-GHz channels, Journal of Geophysical Research: Oceans, 113, 2008.

Szczodrak, M., Minnett, P. J., and Gentemann, C.: Long Term Comparison of AMSR-E Retrievals and Ship Based Measurements of Total Water Vapor in the Caribbean Sea, AGU Fall Meeting Abstracts, 2005.

Szczodrak, M., Minnett, P. J., and Gentemann, C.: Comparison of AMSR-E Retrievals of Total Water Vapor over the Ocean with Ship based Measurements, 10th Symposium on Integrated Observing and Assimilation Systems for the Atmosphere, Oceans, and Land Surface (IOAS-AOLS), 2006.

Tonboe, R., Andersen, S., and Toudal, L.: Anomalous winter sea ice backscatter and brightness temperatures, Danish meteorological institute scientific report no. 03-13, p. 59., Danish Meteorological Institute, 2003.

Trenberth, K. E., Fasullo, J., and Smith, L.: Trends and variability in column-integrated atmospheric water vapour, Climate Dynamics, 24, 741–758, 2005.

Vey, S., Dietrich, R., Johnsen, K., Miao, J., and Heygster, G.: Comparison of tropospheric water vapour over antarctica derived from AMSU-B data, ground-based GPS data and the NCEP/NCAR

reanalysis, JOURNAL OF THE METEOROLOGICAL SOCIETY OF JAPAN, 82, 259 – 267, doi:10.2151/jmsj.2004.259, 2004.

Wang, J., Racette, P., and Triesky, M.: Retrieval of precipitable water vapour by the millimeter-wave imaging radiometer in the arctic region during FIRE-ACE, IEEE Trans. Geosci. Remote Sens., 39, 595–605, 2001.

Wentz, F. J.: A well-calibrated ocean algorithm for special sensor microwave / imager, J. Geophys. Res., 102(C4), 881–894, doi:10.1029/96JC01751, 1997.

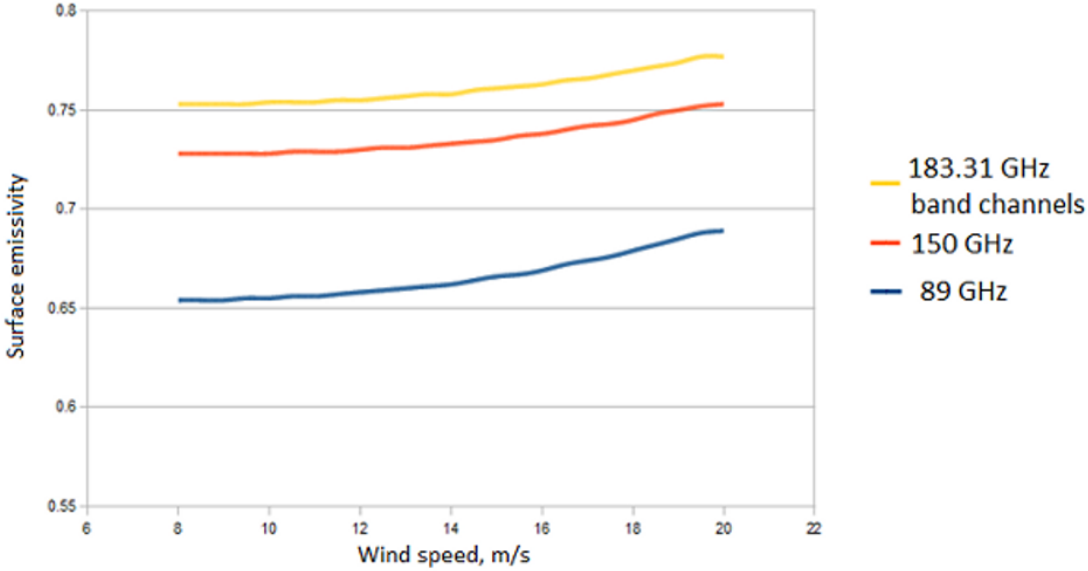

Fig. 1. Ocean surface emissivities' dependence on wind speed.

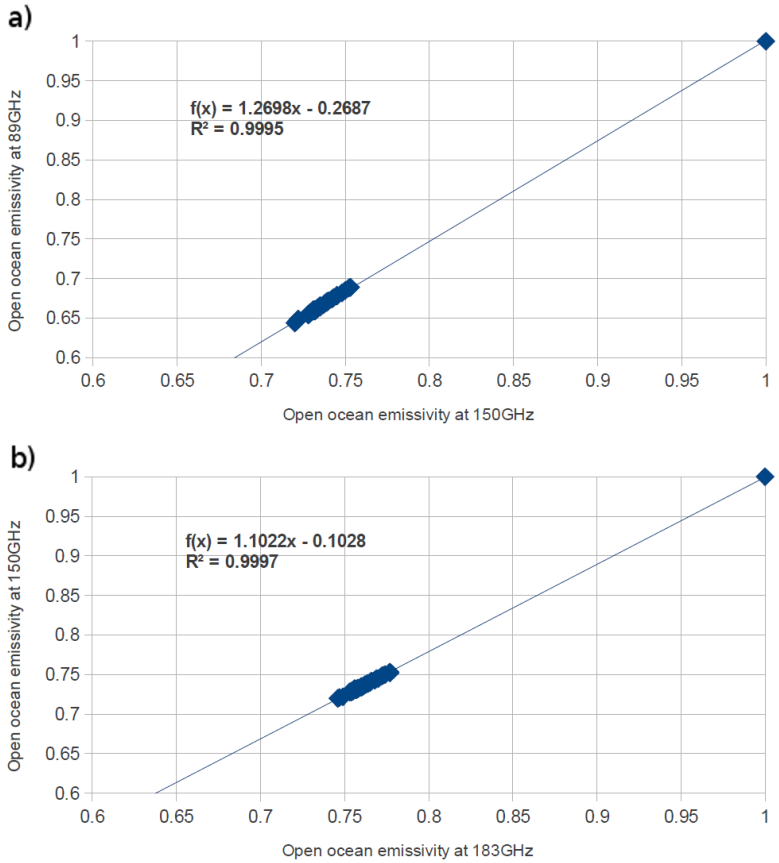

Fig. 2. Regression plot for ocean surface emissivity at 89 and 150 GHz (~~top~~panel a) and at 150 and 183 GHz (~~bottom~~panel b).

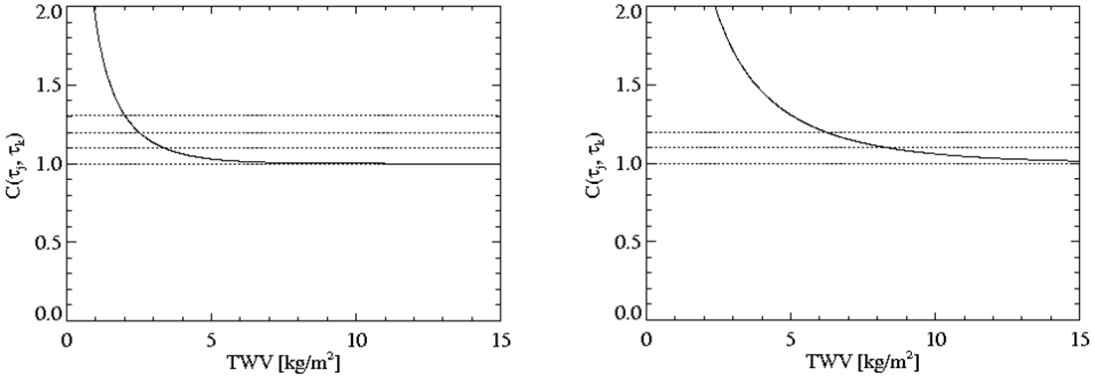

Fig. 3. $C(\tau_j, \tau_k)$) parameter for mid-TWV algorithm (left) and for extended-TWV algorithm (right). The dashed horizontal lines represent the variability interval for the $C(\tau_j, \tau_k)$) parameter inside the TWV range corresponding to each case.

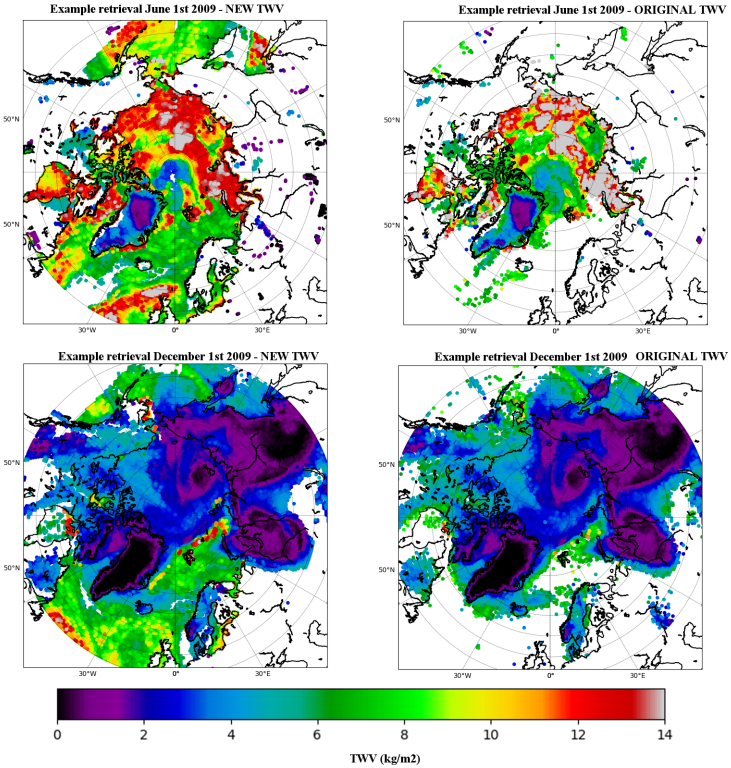

Fig. 4. ~~1st of June 2009,~~ Daily TWV maps of the ~~Arctic~~ Northern Hemisphere obtained from the ~~New~~ new algorithm (~~bottom~~ left column), compared to ~~ECMWF model data (top), and TWV map from~~ the ~~Original~~ original AMSU-B algorithm (~~bottom~~ right column). The days represented here are 1st of June 2009 for the top row, and 1st of December 2009 for the bottom row.

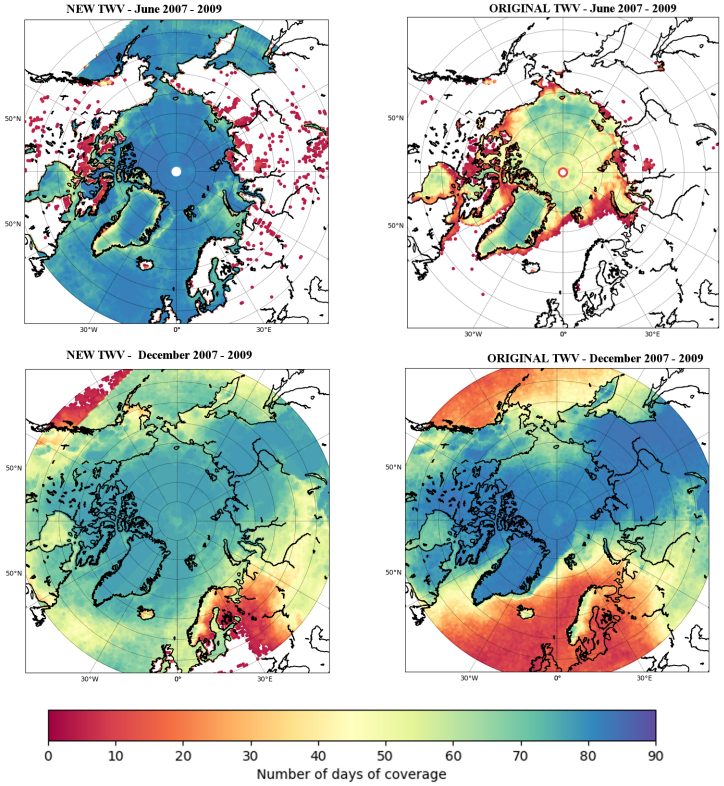

Fig. 5. Number of days of coverage for the Northern Hemisphere for one typical summer and one winter month, over three years. The top row represents the month of June for the 2007-2009 interval, while the bottom row is December for the same three years. The left side column shows results for the new algorithm, while the right side for the original AMSU-B algorithm.

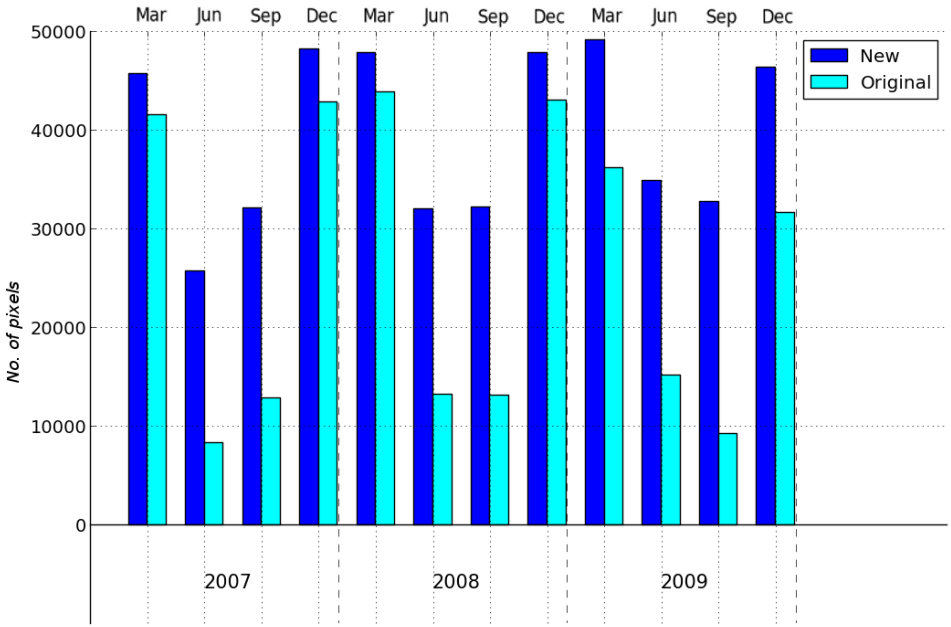

Fig. 6. ~~Average~~ Monthly average number of pixels covered by each method for the test interval of three years.

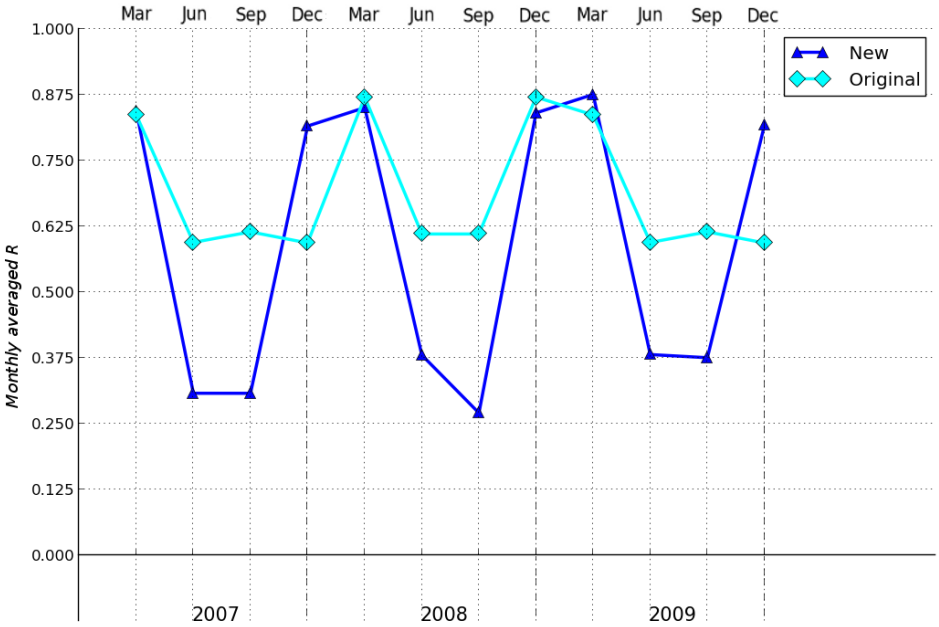

Fig. 7. Correlation ~~of Original~~ for the original and ~~New~~ the new AMSU-B TWV retrieval ~~versus~~ with ECMWF data.

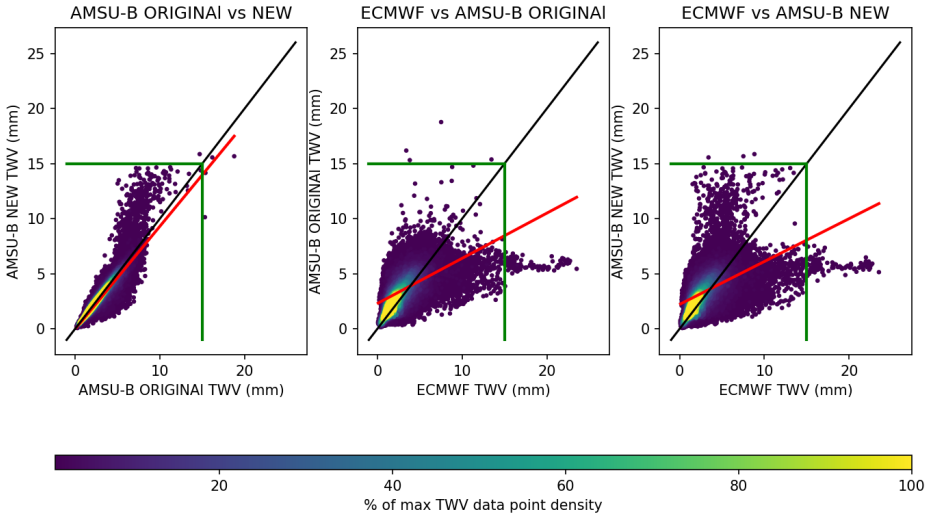

Fig. 8. Scatter plots of the original and new AMSU-B TWV retrievals vs ECMWF TWV. The spatial domain is the common valid domain of both methods. The entire test dataset of 12 months over three years is represented. The black line is the identity line, while the red line represents the data linear regression and the two green lines show the 15(kg/m^2) saturation limit of the extended range TWV retrieval module.

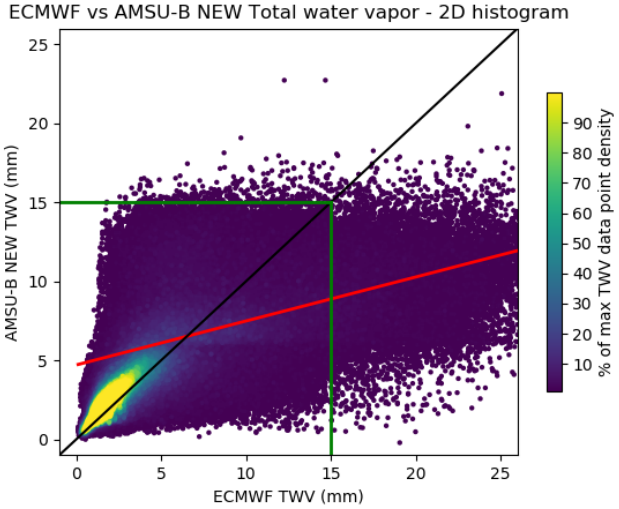

Fig. 9. New AMSU-B TWV retrieval vs ECMWF TWV. The spatial domain is the full valid domain of the new algorithm. The entire test dataset of 12 months over three years is represented. The black line is the identity line, while the red line represents the data linear regression and the two green lines show the 15(kg/m^2) saturation limit of the extended range TWV retrieval module.

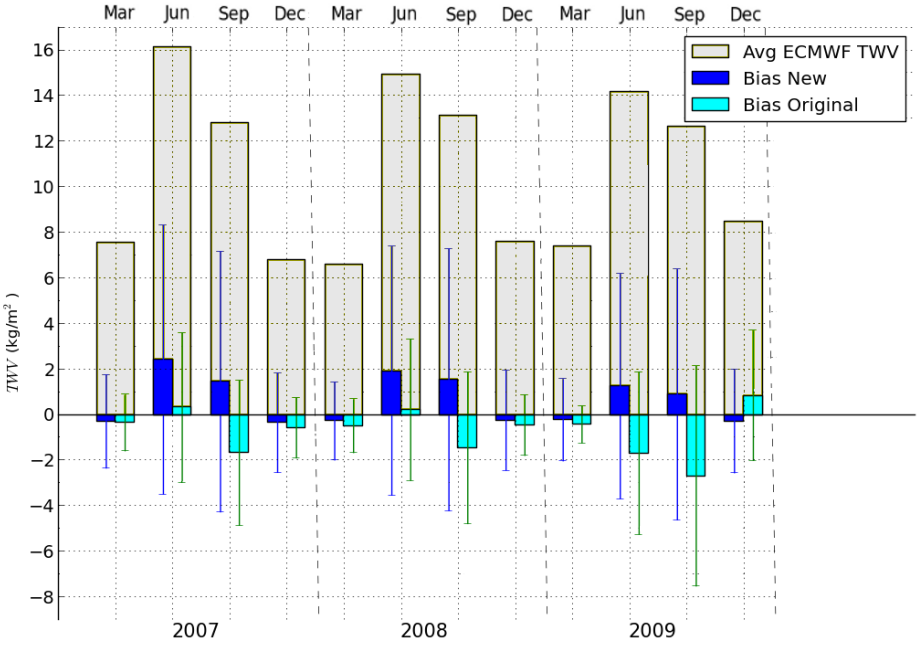

Fig. 10. Bias comparison of the Original and New AMSU-B TWV retrieval versus ECMWF data. Error bars represent ~~RMS~~the RMSD between the retrieved TWV data and ECMWF TWV.

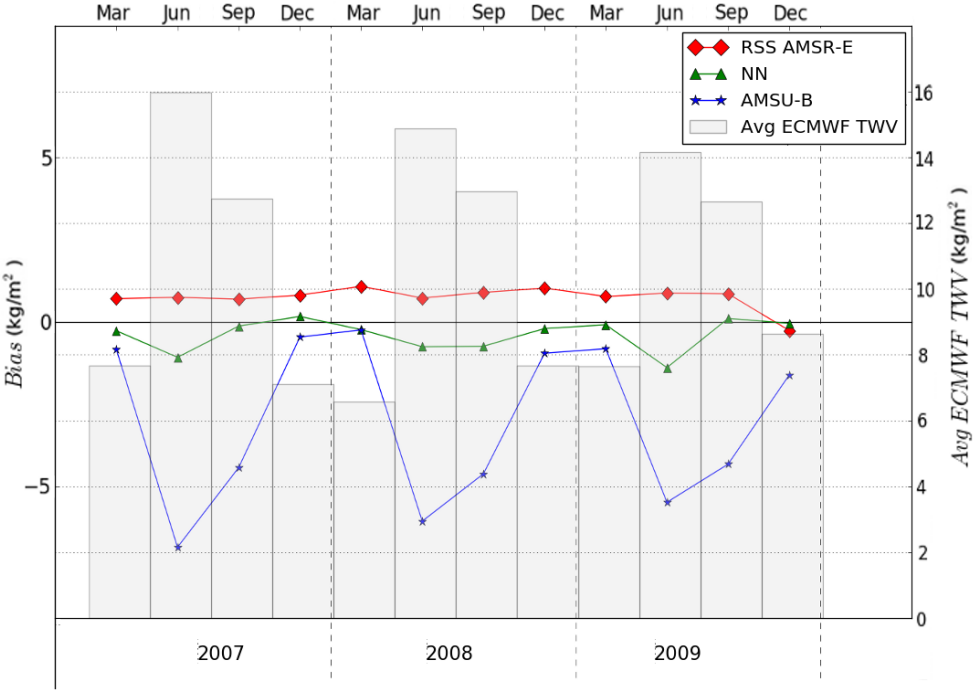

Fig. 11. Bias for the New AMSU-B, AMSR-E ~~global~~ RSS and AMSR-E Neural Network retrievals over open ocean versus ECMWF average TWV value. The curves represent the monthly averaged bias values for each of the three algorithms with the scale on the left side. The vertical columns in the background represent the monthly mean TWV value from ECMWF data with the scale on the right side.

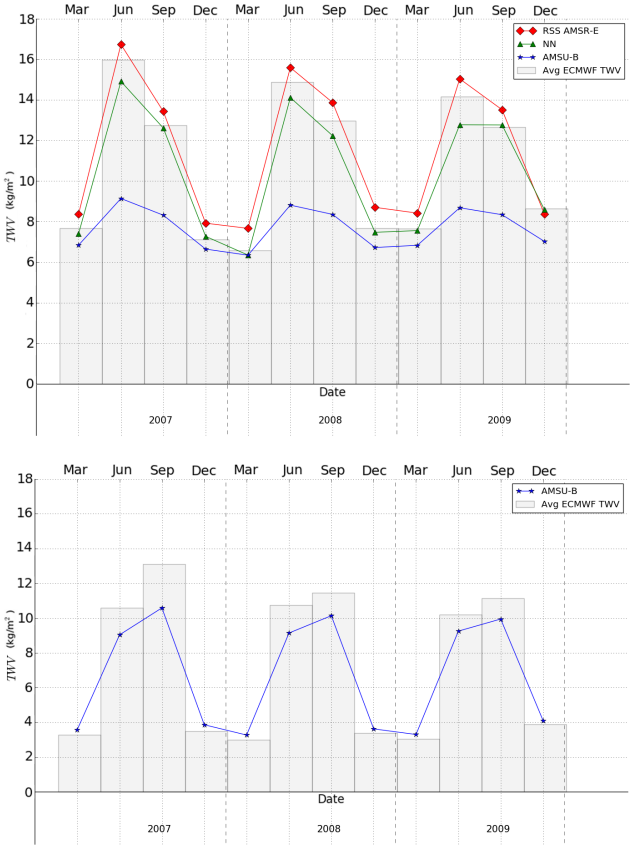

Fig. 12. Average TWV value for the three tested retrievals plotted over ECMWF average TWV value for open ocean areas (top) and New AMSU-B alone plotted over ECMWF average TWV value including all open water, land and sea ice-covered regions of the Arctic where valid values can be retrieved (bottom).The curves represent the monthly averaged TWV values for each algorithm. The vertical columns in the background represent the monthly mean TWV value from ECMWF data.

Table 1. Comparative structure of three TWV retrieval algorithms. SI represents sea ice only and OW - open water as surface types where the individual modules can be applied. L,M and E represent low, mid and respectively extended range TWV retrieval modules. *The Miao algorithm was developed for the SSM/T2 instrument and for the Antarctic region.

Method	Sub-modules	Channel freq. (GHz)	Channel no.	TWV (kg/m^2)	Surface
Miao algorithm	L-TWV	183.31±1,±3,±7	2,3,4*	0 – 1.5	All
	M-TWV	183.31±3,±7,150	3,4,5*	1.5 – 6	All
Original AMSU-B	L-TWV	183.31±1,±3,±7	18,19,20	0 – 1.5	All
	M-TWV	183.31±3,±7,150	19,20,17	1.5 – 7	All
	E-TWV - SI	183.31±7,150,89	20,17,16	7 – 15	SI
New AMSU-B	L-TWV	183.31±1,±3,±7	18,19,20	0 – 1.5	All
	M-TWV	183.31±3,±7,150	19,20,17	1.5 – 7	SI/land
	M-TWV - OW	183.31±3,±7,150	19,20,17	1.5 – 7	OW
	E-TWV - SI	183.31±7,150,89	20,17,16	7 – 15	SI
	E-TWV - OW	183.31±7,150,89	20,17,16	7 – 15	OW